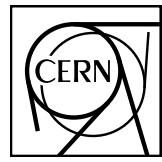


EUROPEAN ORGANIZATION FOR NUCLEAR RESEARCH



May 21, 2017

D-hadron correlations in p-Pb collisions at $\sqrt{s_{NN}} = 5.02 \text{ TeV}$

F. Colamaria, S. Kumar, M. Mazzilli

Abstract

In this note, we present the analysis of azimuthal correlations of D mesons and primary charged particles performed in the ALICE central barrel in p-Pb collisions at $\sqrt{s_{NN}} = 5.02 \text{ TeV}$, from 2016 data taking, in an extended p_T range and with additional observables with respect to p-Pb 2013 data analysis. After a description of the analysis strategy, corrections and systematic uncertainties, the results obtained for prompt D^0 , D^{*+} and D^+ mesons in different ranges of transverse momentum of the D meson and of the associated particles are presented and compared to Monte Carlo models and, for the common p_T ranges and observables, to 2013 p-Pb analysis.

1 Contents

2	1 Introduction and Motivation	2
3	2 Data/Monte Carlo samples and event selection	3
4	3 Analysis strategy	4
5	3.1 Code used for the analysis	7
6	3.2 Corrections	7
7	3.2.1 Event Mixing	7
8	3.2.2 Tracking and D-meson trigger efficiency	9
9	3.2.3 Beauty feed-down	11
10	4 Systematic uncertainties and checks of analysis consistency	12
11	5 Results	13
12	5.1 Comparing the three D meson correlation distributions	13
13	5.2 Average of D^0 , D^+ and D^{*+} results	13
14	5.3 Nearside associated yield, nearside width and baseline as function of the D meson p_T	20
15	5.3.1 Results for near-side yield, near-side width and baseline	24
16	6 Conclusions	38
17	7 Bibliography	39

18 **1 Introduction and Motivation**

19 The study of the azimuthal correlations of heavy-flavoured particles and charged particles at the LHC
 20 energies provides a way to characterize charm production and fragmentation processes in pp collisions
 21 as well as a way to probe our understanding of QCD in the perturbative regime, accessible in a large
 22 kinematic range given the large mass of heavy quarks. Flavour conservation in QCD implies that charm
 23 quarks are always produced as pairs of quarks and anti-quarks. The azimuthal correlations obtained
 24 using a meson carrying a heavy quark as trigger particle with the other charged particles in the same
 25 event give the possibility to study the underlying charm production mechanism in detail. In particular,
 26 prompt charm quark-antiquark pair production leads back to back in azimuth at first order in leading-
 27 order perturbative-QCD (pQCD). Heavy quarks produced from the splitting of a massless gluon can be
 28 rather collimated and may generate sprays of hadrons at small $\Delta\phi$. Finally, for hard-scattering topologies
 29 classified as “flavour-excitation”, a charm quark undergoes a hard interaction from an initial splitting
 30 ($g \rightarrow c\bar{c}$), leading to a big separation in rapidity of the hadrons originating from the antiquark (quark)
 31 with respect to the trigger D meson and contribute to a rather flat term to the $\Delta\phi$ -correlation distribution.

32 Heavy-flavour correlation studies in more complex collisional systems, like Pb-Pb, play a crucial role in
 33 studying the modification of the fragmentation of charmed jets due to in-medium (or cold nuclear matter,
 34 in case of p-Pb collisions) effects, in a similar way as it was done for di-hadron correlation studies in
 35 heavy-ion collisions (see for example [4, 5]). Furthermore, the recent observation of long range cor-
 36 relations in p-Pb for light flavour hadrons and for heavy-flavour decay electrons [1] points to possible
 37 collective effects or effects originating from gluon saturation in the initial state. More information could
 38 be extracted by the eventual observation of the same effect with D mesons.

39

40 In the following, we describe the analysis strategy for p-Pb in all its steps, and we describe the list
 41 of corrections and the estimation of the systematic uncertainties done. We then present the results of
 42 $\Delta\phi$ correlations, and quantitative observable extracted to fits to those distributions, obtained for prompt
 43 D^0 , D^+ and D^{*+} in different ranges of transverse momentum for the D-meson (trigger particle) and the
 44 associated particles.

45 **2 Data/Monte Carlo samples and event selection**

46 The data samples used for the analyses were the FAST and CENT_woSDD samples from periods LHC16q
 47 and LHC16t (merged AOD samples). The reason for this choice is explained later on. It was verified, by
 48 looking at D-meson and track η and ϕ distributions, and at the mixed-event correlation distributions for
 49 each subsamples, that no visible differences arose for the four periods, hence it was possible to perform
 50 the analysis directly on the merged samples without any bias.

51 The Monte Carlo productions adopted for this study were:

- 52 1. LHC17d2a_fast_new, a HIJING production with enrichment, for each event, of c OR b quarks
 53 and their decay chains, performed by PYTHIA6 with Perugia2011 tune, and with forced hadronic
 54 decays of the charmed hadrons. This production was used for D-meson efficiency evaluation,
 55 purity estimation and Monte Carlo closure test.
- 56 2. LHC17a2b_cent_woSDD and LHC17a2b_fast, minimum-bias productions perfomed with DPM-
 57 JET generator, used for the evaluation of the tracking efficiency.

58 Table 1 shows the list of runs used for the analysis, for each of the data taking periods, and of the Monte
 59 Carlo productions used to evaluate the corrections:

60 The trigger mask request for the event selection is kINT7. Only events with a reconstructed primary
 61 vertex within 10 cm from the centre of the detector along the beam line are considered for both pp
 62 and pPb collisions. This choice maximises the detector coverage of the selected events, considering
 63 the longitudinal size of the interaction region, and the detector pseudorapidity acceptances. For pPb
 64 collisions, the center-of-mass reference frame of the nucleon-nucleon collision is shifted in rapidity by
 65 $y_{NN} = 0.465$ in the proton direction with respect to the laboratory frame, due to the different per-nucleon
 66 energies of the proton and the lead beams. Beam-gas events are removed by offline selections based
 67 on the timing information provided by the V0 and the Zero Degree Calorimeters, and the correlation
 68 between the number of hits and track segments in the SPD detector. This is automatically performed in
 69 the Physic Selection, a positive outcome of which is required during our event selection. The minimum-
 70 bias trigger efficiency is 100% for events with D mesons with $p_T > 1$ GeV/c. For the analyzed data
 71 samples, the probability of pile-up from collisions in the same bunch crossing is below 2% per triggered
 72 event (in most of the runs, well below 1%). Events in which more than one primary interaction vertex
 73 is reconstructed with the SPD detector (with minimum of 5 contributors, and a z distance greater than
 74 0.8 cm) are rejected, which effectively removes the impact of in-bunch pile-up events on the analysis.
 75 Out-of-bunch tracks are effectively rejected by the request of at least one point in the SPD, which has
 76 a very limited time acquisition window (300 ns). Indeed, though the default associated track selection
 77 requires a minimum of 2 points in the ITS, as it will be shown later on full compatibility of the corrected
 78 results with 2 and 3 minimum ITS clusters is obtained. For FAST and CENT_woSDD samples, the latter
 79 case indirectly forces the presence of a point in the SPD.

80 **A SMALL DISCUSSION FOR wsdd VS wosdd SAMPLES MUST BE DONE, WITH THE REA-
 81 SONING OF OUR FINAL CHOICE (WITH PLOTS FOR AT LEAST ONE MESON, BUT BET-
 82 TER BOTH D+ and D*). YOU CAN PICK THE PLOTS FROM SHYAM AND MARIANNA'S
 83 TALKS!!**

Type	Production	Run list	nEvents
Monte-Carlo	LHC17d2a_fast_new/AOD (c/b enriched), LHC17a2b_fast (MB), LHC17a2b_cent_woSDD (MB)	265525, 265521, 265501, 265500, 265499, 265435, 265427, 265426, 265425, 265424, 265422, 265421, 265420, 265419, 265388, 265387, 265385, 265384, 265383, 265381, 265378, 265377, 265344, 265343, 265342, 265339, 265338, 265336, 265335, 265334, 265332, 265309, 267165, 267164, 267163, 267166 = [22 runs]	?M
Data	“LHC16q, pass1_CENT_woSDD/AOD” “LHC16q, pass1_FAST/AOD” “LHC16t, pass1_CENT_woSDD/AOD” “LHC16t, pass1_FAST/AOD”	265525, 265521, 265501, 265500, 265499, 265435, 265427, 265426, 265425, 265424, 265422, 265421, 265420, 265419, 265388, 265387, 265385, 265384, 265383, 265381, 265378, 265377, 265344, 265343, 265342, 265339, 265338, 265336, 265335, 265334, 265332, 265309 = [32 runs] 265525, 265521, 265501, 265500, 265499, 265435, 265427, 265426, 265425, 265424, 265422, 265421, 265420, 265419, 265388, 265387, 265385, 265384, 265383, 265381, 265378, 265377, 265344, 265343, 265342, 265339, 265338, 265336, 265335, 265334, 265332, 265309 = [32 runs] 267166, 267165, 267164, 267163 = [4 runs] 267166, 267165, 267164, 267163 = [4 runs]	261M total 260M 40M 41M

Table 1: Data Set and Run list

84 3 Analysis strategy

85 The analysis strategy follows the one used from 2013 p-Pb data sample. Correlation pairs are formed
 86 by trigger particles (D mesons) reconstructed and selected in the following p_T^{trig} ranges: $3 < p_T^{\text{trig}} < 5$,
 87 $5 < p_T^{\text{trig}} < 8$, $8 < p_T^{\text{trig}} < 16$, $16 < p_T^{\text{trig}} < 24 \text{ GeV}/c$, and associated particles (charged tracks) for the
 88 following p_T^{assoc} regions: $p_T^{\text{assoc}} > 0.3$, $0.3 < p_T^{\text{assoc}} < 1$, $1 < p_T^{\text{assoc}} < 2$, $2 < p_T^{\text{assoc}} < 3$, $p_T^{\text{assoc}} > 3 \text{ GeV}/c$
 89 (with the addition of $p_T^{\text{assoc}} > 1 \text{ GeV}/c$ for comparison with p-Pb 2013 results). In D meson correla-
 90 tions, the particle identification defines the trigger particle rather than a momentum cut and therefore
 91 the momentum range of the associated particles is not constrained by that of the trigger particle. Our
 92 definition of associated particle includes any charged particle coming from the primary vertex of interac-
 93 tion, including those coming from strong and electromagnetic decay of unstable particles, and particles
 94 deriving from the decay of hadrons with charm or beauty. We therefore include any charged particle
 95 except those coming from weak decays of strange particles and particles produced in the interaction
 96 with the detector material. This definition corresponds to that used in the method `AliAODMCParticle::IsPyphysicalPrimary()`. All associated particles surviving the selection cuts and not matching the
 97 adopted criterion are considered as a contamination whose contribution has to be corrected for.
 98

99

100 The analysis is performed through the following steps:

- 101 1. **D meson selection and signal extraction.** For each single event, “trigger” particles are defined
 102 as the selected D meson candidates (D^0 , D^+ and D^{*+}) within a given p_T^{trig} range. The detection
 103 strategy for D mesons at central rapidity is the same as that described in [6] and is based on the
 104 reconstruction of decay vertices displayed from the primary vertex by a few hundred μm and on
 105 the identification of the decay-particle species. The identification of the charged kaon and pion in
 106 the TPC and TOF detectors helps to further reduce the background at low p_T . An invariant-mass
 107 analysis is then used to extract the raw signal yield, using the same fit functions described in [6].
 108 The D mesons are selected in the rapidity range varying from $|y| < 0.5$ at low p_T to $|y| < 0.8$ for
 109 $p_T > 5 \text{ GeV}/c$.

- 110 2. **Correlation of D candidates with associated tracks.** Particle pairs are formed by associating each
 111 trigger particle with the charged primary particles passing the track selection (excluding those
 112 coming from the decay of the D-meson candidate) in a specified p_T^{assoc} interval (which can overlap
 113 with the p_T^{trig} range) and in the pseudo-rapidity range $|\eta| < 0.8$. For the D^0 meson, also the low-
 114 momnetum pion tracks from feed-down of D^{*+} mesons are removed via 3σ invariant mass cut on
 115 the $M(K\pi\pi) - M(K\pi)$ difference. This because these soft pion are not related to the charm quark
 116 fragmentation chain. For D meson candidates in the invariant mass signal region, defined by a \pm
 117 2σ interval around the D meson mass, the azimuthal angle difference $\phi^{\text{assoc}} - \phi^{\text{trigg}} \equiv \Delta\phi$ and the
 118 pseudorapidity difference $\eta^{\text{assoc}} - \eta^{\text{trig}} \equiv \Delta\eta$ are evaluated and stored to build two-dimensional
 119 correlation distribution.

120 ADD: CUT OPTIMIZATION PARAGRAPH FOR D0, WITH SOME PLOT- PUT A REFER-
 121 ENCE TO MY LAST CUT OPT TALK, ON 22 MARCH HFCJ; CUT MODIFICATIONS (JUST
 122 AS TEXT, OR WITH 1-2 PLOTS) FOR D+; SAY THAT D+ HAS STD D''H p-Pb 2013 CUTS
 123 INSTEAD

- 124 3. **Correction for limited acceptance and detector inhomogeneities with Event Mixing** The angular
 125 correlation distribution may be affected, even for uncorrelated pair of particles, by structures
 126 not due to physical effects, but originating from the limited detector acceptance, as well as from
 127 angular inhomogeneities in the trigger and track reconstruction efficiencies as a function of $\Delta\phi$ and
 128 $\Delta\eta$. Effects of this kind are removed using the Event Mixing technique. In details, the analysis
 129 is executed on the same data sample of the standard one (called “same event” analysis, SE), but
 130 the trigger particles found in each event are correlated to charged particles reconstructed in differ-
 131 ent events (“Mixed Events” analysis, ME) with similar characteristic, in particular concerning the
 132 event multiplicity and z position of the primary vertex (see Section 3.2.1).

133
 134 The differential yield of associated particles per trigger particle is obtained by

$$\frac{1}{N_{\text{trig}}} \frac{d^2N^{\text{pair}}}{d\Delta\eta d\Delta\phi} = B_{ME}(0,0) \times \frac{S(\Delta\eta, \Delta\phi)}{B_{ME}(\Delta\eta, \Delta\phi)}, \quad (1)$$

135 where N^{pair} is the total number of correlated D-hadron pairs. The functions $S(\Delta\eta, \Delta\phi)$ and $B_{ME}(\Delta\eta, \Delta\phi)$
 136 are the signal and the mixed event background distributions, respectively. The latter is normalized
 137 to its value in $(\Delta\eta, \Delta\phi) = (0,0)$, i.e. $(B(0,0))$. Further details on the mixed-event correction are
 138 provided further on.

139 The signal distribution is the per-trigger-particle yield of pairs found in the same event,

$$S(\Delta\eta, \Delta\phi) = \frac{1}{N_{\text{trig}}} \frac{d^2N^{\text{same}}}{d\Delta\eta d\Delta\phi}, \quad (2)$$

140 where N^{same} is the number of such pairs within a $(\Delta\eta, \Delta\phi)$ bin, divided by the product of the $\Delta\eta$
 141 and $\Delta\phi$ bin widths.

142 The background distribution from mixed-event is given by

$$B_{ME}(\Delta\eta, \Delta\phi) = \frac{1}{N_{\text{trig}}} \frac{d^2 N^{\text{mix}}}{d\Delta\eta d\Delta\phi}, \quad (3)$$

143 where N^{mix} denotes the number of mixed-event pairs. The ratio $B(0,0)/B(\Delta\eta, \Delta\phi)$ determines
 144 the pair acceptance correction factor. Multiplying the signal distribution by this ratio gives the
 145 acceptance-corrected per-trigger-particle associated yield.

- 146 4. **Subtraction of background correlation from signal distribution.** The invariant mass signal re-
 147 gion includes also background D-meson candidates. Their contribution to the raw correlation
 148 distribution is subtracted as follows. For each p_T bin, the mean and the sigma of the invariant
 149 mass spectrum are extracted. For D^0 and D^+ , a “background” region is defined in the sidebands
 150 of the mass distribution as the interval $4\text{GeV}/c^2 < |m - m^{\text{pdg}}| < 8\text{GeV}/c^2$ (for the D^{*+} meson,
 151 only the right sideband is used). The angular correlation distribution for background candidates
 152 in this region is extracted and normalized with respect to the background in the signal region es-
 153 timated from the mass fit. This normalized background correlation distribution is then subtracted
 154 from the raw signal one to obtain the signal correlation distribution. The normalization factor is
 155 the ratio of the number of background candidates under the signal peak (obtained bin-counting the
 156 candidates in the signal region and subtracting the integral of the fit function for the signal only, in
 157 the same range¹ **NOTE: THIS, AT LEAST FOR D0, SHALL BE REVERSED, SINCE WITH**
 158 **OPTIMIZED CUTS S > B IN MOST BINS. FOR D+ AND D*, PLEASE CHECK!!!**) over the
 159 number of background candidates in the sidebands (obtained via bin-counting in the sideband re-
 160 gion). This normalized background correlation distribution is then subtracted from the raw signal
 161 one to obtain the signal correlation distribution.

162 ADD PLOT OF 1D SIGNAL, SB, SIGNAL-SB REGION (I UPLOADED ONE EXAMPLE FOR
 163 D0)

- 164 5. **Correction for D meson efficiency and associated track efficiency.** After filling the signal and
 165 background correlation distributions, it is necessary to take into account also for the correlations
 166 with tracks not reconstructed, or not passing the quality selection due to poor reconstruction. In
 167 the same way, the loss of D-mesons which are not reconstructed, or do not pass the selection, im-
 168 impacts the correlation distribution shape. Hence, each pair is weighted by the inverse of the product
 169 of the associated track and D meson reconstruction efficiency, ε_{trk} and $\varepsilon_{\text{trig}}$. The associated track
 170 efficiency dependence on the particle pseudorapidity, transverse momentum, and z-coordinate of
 171 the primary vertex is taken into account. For the trigger particle efficiency only the p_T and the
 172 event multiplicity dependencies of the efficiency are considered, mainly to avoid large statistical
 173 fluctuations on the efficiency values arising when including also the dependency on η , due to the
 174 limited size of the Monte Carlo sample from which the D meson efficiencies are evaluated. The
 175 details of the efficiency corrections can be found in the following sections. To properly count the
 176 number of trigger particles used to normalize the correlation distributions, N_{trig} , each D meson is
 177 weighted with the inverse of its efficiency in the invariant mass distribution. The main role of the
 178 correction for the D meson efficiency is to account for the p_T dependence of the correlation distri-
 179 bution within a given D meson p_T interval. Indeed, only the p_T shape of the D meson efficiency
 180 within the correlation p_T^{trig} ranges is relevant while the average value in the p_T range is simplified
 181 due to the normalization of the correlation distribution to the number of trigger particles.

- 182 6. **Projection in $\Delta\phi$.** The limited statistics available does not allow to study the two dimensional
 183 $(\Delta\eta, \Delta\phi)$ distribution, which is therefore projected to the $\Delta\phi$ axis by integrating on $|\Delta\eta| < 1$. De-
 184 spite, in principle, our maximum $\Delta\eta$ acceptance is of $|\Delta\eta| < 1.6$, removing the large $|\Delta\eta|$ regions

¹With this procedure, the statistical fluctuations in the signal region are treated as background fluctuations. This is acceptable, since in most of the p_T ranges $B > S$, hence B fluctuations are higher than S fluctuations.

allow us to reject angular regions with very low statistics, where fluctuations would be amplified by a large mixed-event correction, and avoid the so-called wings effect.

As the difference in the azimuthal angle is periodic ($\Delta\phi = 0 = 2\pi$), the $\Delta\phi$ -range is limited to the essential range of 2π . The $\Delta\phi$ -limits are chosen to be $[-\pi/2, 3\pi/2]$ in order to provide a good visibility of the correlation pattern, which peaks around 0 and π .

- 185 allow us to reject angular regions with very low statistics, where fluctuations would be amplified
186 by a large mixed-event correction, and avoid the so-called wings effect.
- 187 As the difference in the azimuthal angle is periodic ($\Delta\phi = 0 = 2\pi$), the $\Delta\phi$ -range is limited to
188 the essential range of 2π . The $\Delta\phi$ -limits are chosen to be $[-\pi/2, 3\pi/2]$ in order to provide a good
189 visibility of the correlation pattern, which peaks around 0 and π .
- 190 7. **Correction for the contamination of secondary particles** The DCA to primary vertex cut, ap-
191 plied during the associated track selection, has the role of removing the secondary particles from
192 the associated track sample. Secondary particles are indeed produced either from long-lived
193 strange hadrons or from interaction of particles with the detector material. A residual contamina-
194 tion from secondary tracks is hence expected in the correlation distributions. This contamina-
195 tion is estimated from Monte Carlo simulation based on Pythia as described more in detail in the next
196 section. The background-subtracted event-mixing corrected correlations are multiplied by a purity
197 factor to remove this contribution.
- 198 8. **Correction for feed-down of D meson from b-hadron decay** The selection strategy employed
199 for the D meson candidates selection enhances the fraction of reconstructed D mesons coming
200 from the decay of a b-hadron. Typical values, with the cuts used for the D-meson selection, are of
201 the order of 10% or less. The correlation distribution of these secondary D mesons will be sensi-
202 tive to the properties of beauty jets and beauty hadron decay, which in general differ from those
203 relative to charm jets and hadrons. The procedure used to subtract this contribution is described in
204 the next section.
- 205 9. **Study of correlation properties.** The properties of the azimuthal correlation distribution are quan-
206 tified by fitting the distribution with a function composed of two Gaussian functions, modelling
207 the near and the away side peaks, and a constant term describing the baseline. The mean of the
208 Gaussian are fixed at $\Delta\phi = 0$ and $\Delta\phi = \pi$. To accomplish the 2π periodicity of the $\Delta\phi$ variable, the
209 Gaussian functions are “duplicated” with mean at $\Delta\phi = 2\pi$ and $\Delta\phi = -\pi$. The fitting procedure
210 is described in details the 5 section.

211 3.1 Code used for the analysis

212 The code used for D meson-hadron correlation analysis is fully committed in AliPhysics. The anal-
213 ysis classes can be found in \$ALICE_ROOT/PWGHF/correlationHF/. The D meson specific classes
214 where the aforementioned steps are carried out are AliAnalysisTaskDStarCorrelations, AliAnalysis-
215 TaskSEDOCorrelations and AliAnalysisTaskDplusCorrelations. The classes which are common to the D
216 meson specific analysis which includes the associated particle cuts and the correlation observables are Al-
217 iHFAssociatedTrackCuts, AliHFCorrelator, AliHFOfflineCorrelator, AliReducedParticle and AliDhCor-
218 relationExtraction. Several additional classes and macros in the same folder deal with the correction
219 steps.

220 3.2 Corrections

221 3.2.1 Event Mixing

222 The event-mixing technique is used for correcting the raw correlation distribution for effects arising
223 from the detector limited acceptance in rapidity and detector spatial inhomogeneities. The calculation
224 of the Event Mixing correlation distribution is performed online. An event pool is created, where events
225 preceding the one containing a D candidate are stored based on their properties (position of the vertex
226 along the z axis and multiplicity). Each time a D meson candidate is found in an event, only the events
227 contained in the same pool as the event under analysis is used to evaluate the correlations for the event
228 mixing correction.

229 For D^0 and D^+ , an offline approach for the mixed-event correction has been developed. In this approach,
 230 D-meson triggers and associated tracks from every analyzed event are stored in dedicated TTree, together
 231 with the needed kinematic information to build correlation distributions, and with identifiers of the events
 232 to which they belong. In this way, it is possible to correlate each D meson with all the tracks belonging
 233 to the same pool over the full event sample, and not being limited to the same subjob as for the online
 234 analysis. This allows to increase the statistics of the mixed-event correlation distributions. It was verified
 235 that online and offline approaches are fully compatible within the statistical uncertainties.

236 The multiplicity and z vertex position bins for the pools used in the p-Pb analysis (for both approaches)
 237 are the following:

- 238 – Multiplicity bins: $(0, 40); (40, 65); (65, +\infty)$
- 239 – Vertex z (cm) = $(-10, -2.5); (-2.5, 2.5); (2.5, 10)$

240 In an ideal case, the mixed event distribution is expected to have a constant flat distribution as function
 241 of $\Delta\phi$ and a triangular shaped distribution in $\Delta\eta$ deriving from the limited η acceptance of the detector.
 242 In case, instead of detector inefficient regions, or holes, in the same angular position for D meson and
 243 associated tracks, these structures produce an excess of correlations at $\Delta\phi = 0$ in the $\Delta\phi$ distribution. The
 244 obtained distribution is used as a weight in each correlation bin, i.e., the corrected correlation distribution
 245 is calculated as follows:

$$\frac{dN^{corr}(\Delta\phi, \Delta\eta)}{d\Delta\phi d\Delta\eta} = \frac{\frac{dN^{SE}(\Delta\phi, \Delta\eta)}{d\Delta\phi d\Delta\eta}}{\frac{dN^{ME}(\Delta\phi, \Delta\eta)}{d\Delta\phi d\Delta\eta}} \frac{dN^{ME}(0, 0)}{d\Delta\phi d\Delta\eta} \quad (4)$$

246 In the previous equation, the last term stands for the average of the bins in the region $-0.2 < \Delta\eta < 0.2$,
 247 $-0.2 < \Delta\phi < 0.2$ (multiple bins are used to minimize the effect of statistical fluctuations on the nor-
 248 malization of the mixed-event plots). This kind of normalization, adopted in the analysis of hadron-
 249 hadron correlations, relies on the fact that at $(\Delta\eta, \Delta\phi) = (0, 0)$ the trigger and associated particle expe-
 250 rience the same detector effects. In the D meson case this is true only on average and not at very low
 251 p_T , since D mesons are reconstructed from particles that can go in different detector region. However,
 252 $(\Delta\eta, \Delta\phi) = (0, 0)$ is in any case the region with maximum efficiency for the pairs (both correlated and
 253 uncorrelated). Thus the same convention was adopted.

254 The mixed-event correlation distributions are built in both D meson signal and sideband regions. Both
 255 are corrected with the relative distributions. An example of the mixed event distribution is shown in
 256 Fig. 1 (middle panels). The expected triangular shape in $\Delta\eta$ addresses the effect of the limited detector
 257 pseudo-rapidity acceptance. Note that the mixed-event distribution is limited to the interval $|\Delta\eta| < 1$: the
 258 decision to limit the mixed-event correction, and thus the whole analysis, to this range was taken in order
 259 to avoid the so-called “wing effect”, i.e. the wing-like structures arising in the correlation distribution at
 large $\Delta\eta$ due to the limited filling of the correlation bins in that region.

Figure 1: $(\Delta\phi, \Delta\eta)$ correlation in the Sidebands and Signal region from Single Event and Mixing Event analysis
 for low p_T : $3 < p_T^{D^+} < 5 \text{ GeV}/c$ with associated track p_T threshold $0.3 \text{ GeV}/c$

Figure 2: $(\Delta\phi, \Delta\eta)$ correlation in the Sidebands and Signal region from Single Event and Mixing Event analysis
 for mid p_T : $5 < p_T^{D^+} < 8 \text{ GeV}/c$ with associated track p_T threshold $0.3 \text{ GeV}/c$

Figure 3: $(\Delta\phi, \Delta\eta)$ correlation in the Sidebands and Signal region from Single Event and Mixing Event analysis
 for high p_T : $8 < p_T^{D^+} < 16 \text{ GeV}/c$ with associated track p_T threshold $0.3 \text{ GeV}/c$

261 Figures 1, 2, 3 show the 2D correlation in Sideband Region and Signal region from SE and ME analysis
 262 for D^+ meson in different p_T region.

263 **3.2.2 Tracking and D-meson trigger efficiency**

264 **(i) Tracking efficiency:** is calculated by obtaining the ratio between the yield at the reconstructed level
265 and generated level, for a defined “type” of particles (in our case non-identified particles) and it is esti-
266 mated differentially in p_T , η , and z_{vtx} of the event.

267 **Implementation :** tracking efficiency maps are produced as TH3D histograms (p_T , η , z_{vtx}) obtained
268 from MC analysis on the minimum-bias samples LHC17a2b_fast and LHC17a2b_cent_woSDD, and ap-
269 plying at reconstructed level the track selections (summarized in Table. 2). These efficiency maps are
270 used in the analysis tasks to extract single track efficiencies; each correlation pairs found in the data anal-
271 ysis is inserted in correlation plots with a weight of **1/efficiency value**. Example plots of the tracking
272 efficiencies as a function of p_T are shown in Fig. ??.

Figure 4: p_T efficiency for standard track selection.

273 Details of cuts at event level and particle selection at different steps are listed in Table. 2 .

MC Generated	
Stages	Cuts
1. MC Part with Generated Cuts	After Event Selection Charge PDG Code Physical Primary Kinematics Cuts $-0.8 < \eta < 0.8$ $pT > 0.3 \text{ (GeV}/c)$
2. MC Part with Kine Cuts	
MC Reconstructed	
4. Reco tracks	After Event Selection Physical Primary Kinematics Cuts $-0.8 < \eta < 0.8$ $pT > 0.3 \text{ (GeV}/c)$ Quality Cuts SetRequireSigmaToVertex(kFALSE) SetDCAToVertex2D(kFALSE) SetMinNCrossedRowsTPC(70) SetMinRatioCrossedRowsOverFindableClustersTPC(0.8) SetMinNClustersITS(3) SetMaxChi2PerClusterTPC(4) SetMaxDCAToVertexZ(1) SetMaxDCAToVertexXY(0.25) SetRequireTPCRefit(TRUE) SetRequireITSRefit(FALSE) Same as step 6
5. Reco tracks with Kine Cuts	
6. MC true with Quality Cuts	
7. Reco tracks with Quality Cuts	

Table 2: Single Track Efficiency cuts detail

274

275 **(ii) D Meson efficiency** - Due to limited statistics, the correlation analysis is performed in quite wide
 276 p_T bins and in each of them the reconstruction and selection efficiency of D mesons is not flat (Fig. 6, 5),
 277 in particular in the lower p_T region. We correct for the p_T dependence of the trigger efficiency within
 278 each p_T -bin. This correction is applied online, by using a map of D meson efficiency as a function of p_T
 279 and event multiplicity (in terms of SPD tracklets in $|\eta| < 1$) extracted from the enriched Monte Carlo
 280 sample LHC17d2a_fast_new. While running the analysis, each correlation entry is weighted by **1/trigger**
 281 **efficiency**. It was observed that multiplicity dependence of the efficiency does not bias the extraction
 282 of the signal yield from the invariant mass distributions (which, as anticipated, are also weighted in the
 283 same manner). Efficiency plots for D^0 , D^+ and D^{*+} mesons are shown in Fig. ??, Fig. 6 and 7.

Figure 5: Top panel: (p_T , multiplicity) dependence (left) and p_T dependence (right) of prompt D^0 meson efficiency. Bottom panels: multiplicity dependence of D^0 meson efficiency for three D^0 p_T ranges: 3-4 GeV/c (left), 5-6 GeV/c (center), 8-12 GeV/c (right). For tracklet multiplicity > 120 , due to the limited statistics, the efficiency value is fixed to the one obtained for $90 < \text{tracklet multiplicity} < 120$.

Figure 6: Top panel: (p_T , multiplicity) dependence of D^+ meson efficiency. Bottom panels: D^+ meson efficiency in multiplicity for three D^+ p_T ranges: 3-5 GeV/ c (left), 5-8 GeV/ c (center), 8-16 GeV/ c (right).

Figure 7: Top panel: (p_T , multiplicity) dependence (left) and p_T dependence (right) of prompt D^{*+} meson efficiency. Bottom panels: multiplicity dependence of D^{*+} meson efficiency for three D^{*+} p_T ranges: 3-4 GeV/ c (left), 5-6 GeV/ c (center), 8-12 GeV/ c (right). For tracklet multiplicity > 120 , due to the limited statistics, the efficiency value is fixed to the one obtained for $90 < \text{tracklet multiplicity} < 120$.

3.2.3 Beauty feed-down

The contribution of correlations of D meson from b-hadron decay is subtracted from the data correlation distributions as:

$$\tilde{C}_{\text{prompt } D}(\Delta\phi) = \frac{1}{f_{\text{prompt}}} \left(\tilde{C}_{\text{inclusive}}(\Delta\phi) - (1 - f_{\text{prompt}}) \tilde{C}_{\text{feed-down}}^{\text{MC templ}}(\Delta\phi) \right). \quad (5)$$

In the above equation, $\tilde{C}_{\text{inclusive}}(\Delta\phi)$ and $\tilde{C}_{\text{prompt } D}(\Delta\phi)$ are per-trigger azimuthal correlation distributions before and after feed-down contribution subtraction, f_{prompt} is the fraction of prompt D meson and $\tilde{C}_{\text{feed-down}}^{\text{MC templ}}$ is a template of the azimuthal correlation distribution for the feed-down component obtained from home-made Monte Carlo simulation at generated level, using PYTHIA6 with Perugia2011 tune. In order to avoid biases related to the different event multiplicity in real and simulated events, the correlation distribution was shifted to have its minimum coinciding with the baseline of the data azimuthal-correlation distribution before feed-down subtraction. The value of f_{prompt} , which depends on D-meson species and varies as a function of the p_T , is estimated on the basis of FONLL predictions for the production of feed-down D mesons at central rapidity, in pp collisions at $\sqrt{s} = 5$ TeV, and using the reconstruction efficiency of prompt and feed-down D mesons, following the so-called N_b approach defined in [6]. Typical values ranges are about 8-10% for the D^0 , about 5% for the D^+ and **XXXX** percent for the D^{*+} . The procedure adopted is the same as what done in pp: however, in p-Pb, in order to consider a possible non-zero v_2 -like modulation of the baseline, a range of $0 < v_2 < 0.2$ values for tracks and for secondary D mesons is considered for the systematic uncertainty evaluation (using an hypothesis of 0 for both cases for central values).

SOME TEMPLATE PLOTS HAVE TO BE ADDED HERE

303 **4 Systematic uncertainties and checks of analysis consistency**

304 **5 Results**

305 **5.1 Comparing the three D meson correlation distributions**

306 To check the compatibility of the three D meson analyses, Figure 9 shows the corrected azimuthal
 307 correlation distributions respectively for D^0 -h, D^{*+} -h and D^+ -h (except for the feed-down subtraction,
 308 on the data sample used in the analysis. Results are shown for $3 < D p_T < 5 \text{ GeV}/c$, $5 < D p_T < 8 \text{ GeV}/c$,
 309 $8 < D p_T < 16 \text{ GeV}/c$ and $16 < D p_T < 24 \text{ GeV}/c$ with associated tracks $p_T > 0.3$, $p_T > 1$, $0.3 < p_T < 1$
 310 GeV/c , $1 < p_T < 2 \text{ GeV}/c$, $2 < p_T < 3 \text{ GeV}/c$ and $p_T > 3 \text{ GeV}/c$.

311 An agreement of the distributions from the three mesons within the uncertainties is found in all the
 312 kinematic ranges.

313 Despite being evaluated in the full 2π range, the range of final results was then reduced to $[0, \pi]$ radians,
 314 reflecting the points outside that range over the value of 0. This allowed to reduce the impact of statistical
 315 fluctuations on the data points (supposing equal statistics for a pair of symmetric bins, after the reflection
 316 the relative statistical uncertainty for the resulting bin is reduced by a factor $1/\sqrt{2}$).

317 **5.2 Average of D^0 , D^+ and D^{*+} results**

318 Given the compatibility within the uncertainties among the D^0 , D^+ and D^{*+} azimuthal correlations, and
 319 since no large differences are visible in the correlation distributions observed in Monte Carlo simulations
 320 based on Pythia with Perugia0, 2010 and 2011 tunes², it was possible to perform a weighted average
 321 (eq. 6) of the azimuthal correlation distributions of D^0 , D^+ and D^{*+} , in order to reduce the overall
 322 uncertainties. Although some correlation between the mesons could be present (about the 30% of the
 323 D^0 , and also part of the D^+ , come from D^{*+} decays), the three selected D-meson samples can be treated
 324 as uncorrelated. The inverse of the sum in quadrature of the statistical uncertainty and of the S and B
 325 extraction uncertainties was used as weight.

$$\left\langle \frac{1}{N_D} \frac{dN_{\text{assoc}}}{dp_T} \right\rangle_{D\text{mesons}} = \frac{\sum_{i=\text{meson}} w_i \frac{1}{N_D} \frac{dN_i^{\text{assoc}}}{d\Delta\phi}}{\sum_{i=\text{meson}} w_i}, w_i = \frac{1}{\sigma_{i,\text{stat}}^2 + \sigma_{i,\text{uncorr.syst}}^2} \quad (6)$$

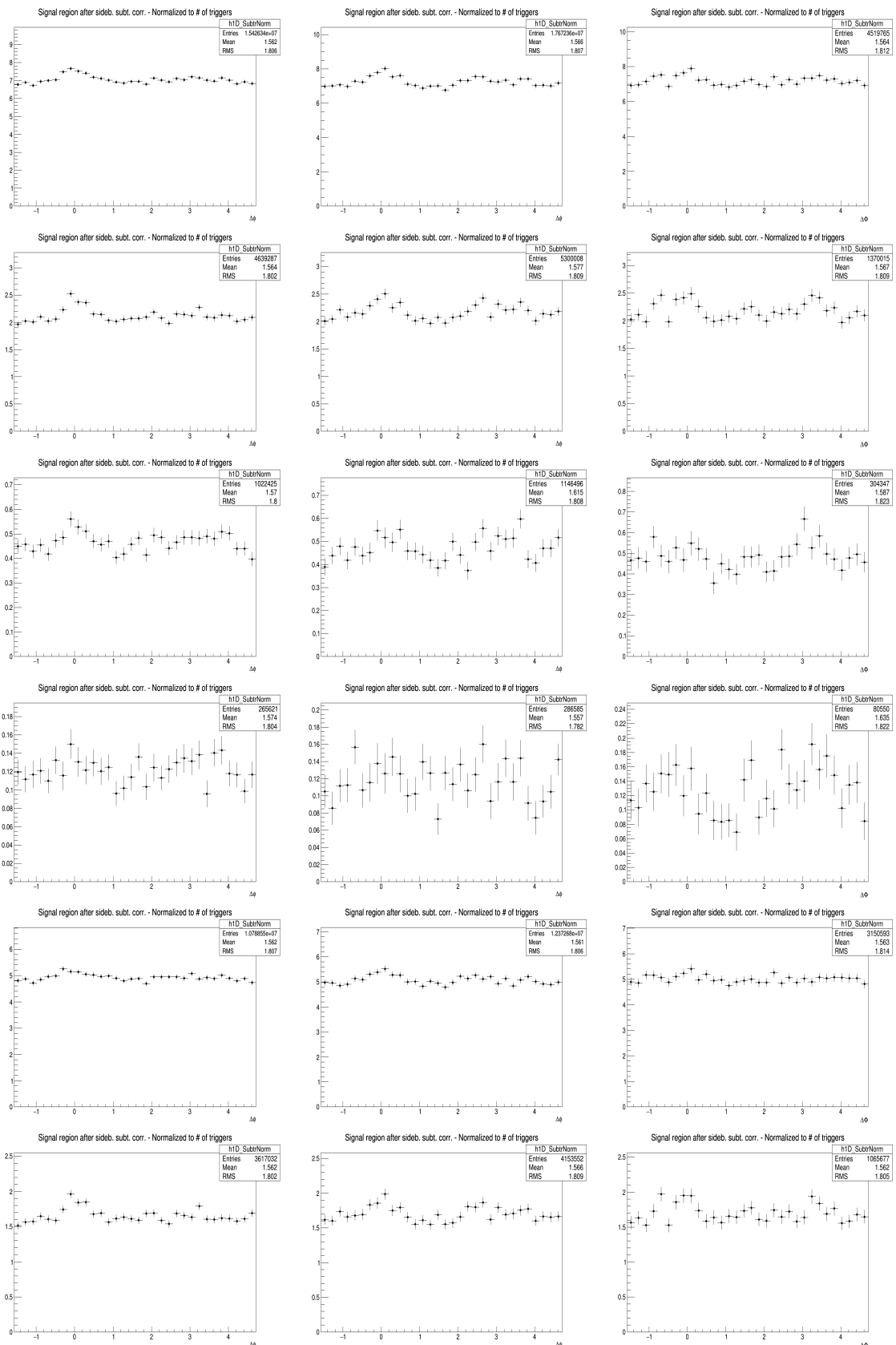
326 The statistical uncertainty and the uncertainty on the S and B extraction on the average were then recal-
 327 culated using the following formula

$$\sigma^2 = \frac{1}{n_D} \frac{\sum_{i=\text{meson}} w_i \sigma_i^2}{\sum_{i=\text{meson}} w_i} \quad (7)$$

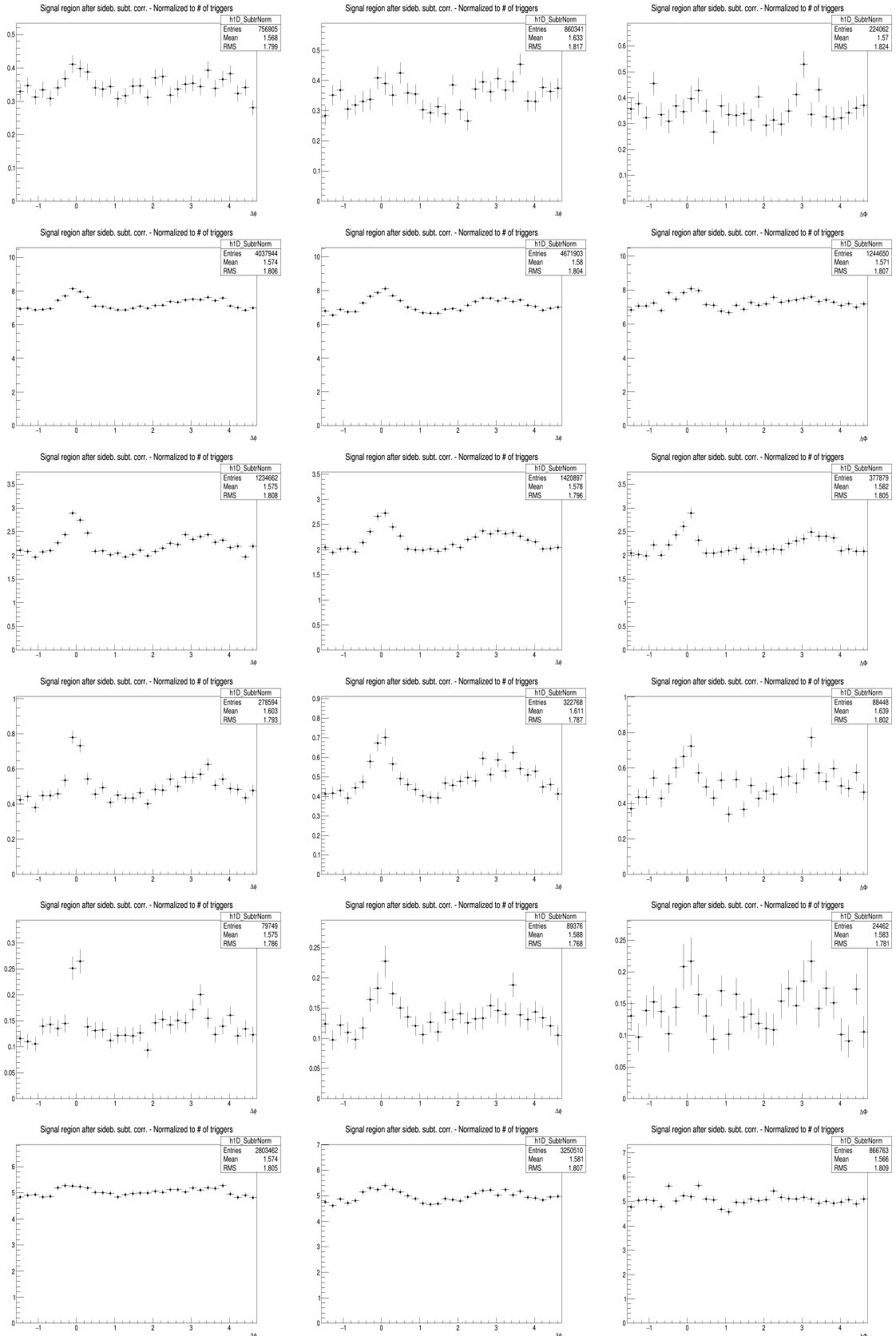
328 where n_D is the number of mesons considered in the average. It can be observed that for $\sigma_i^2 = 1/w_i$ the
 329 formula coincides with the standard one giving the uncertainty on a weighted average. The contribution
 330 to the average systematic uncertainty for those uncertainty sources not included in the weight definition,
 331 was evaluated via error propagation on the formula of the weighted average (6), resulting in equation
 332 (8) and (9) for sources considered uncorrelated and correlated among the mesons. In particular, the
 333 uncertainties on the associated track reconstruction efficiency, on the contamination from secondary, on
 334 the feed-down subtraction, and that resulting from the Monte Carlo closure test were considered fully
 335 correlated among the mesons, while those deriving from the yield extraction (included in the weight
 336 definition) and on the D meson reconstruction and selection efficiency were treated as uncorrelated.

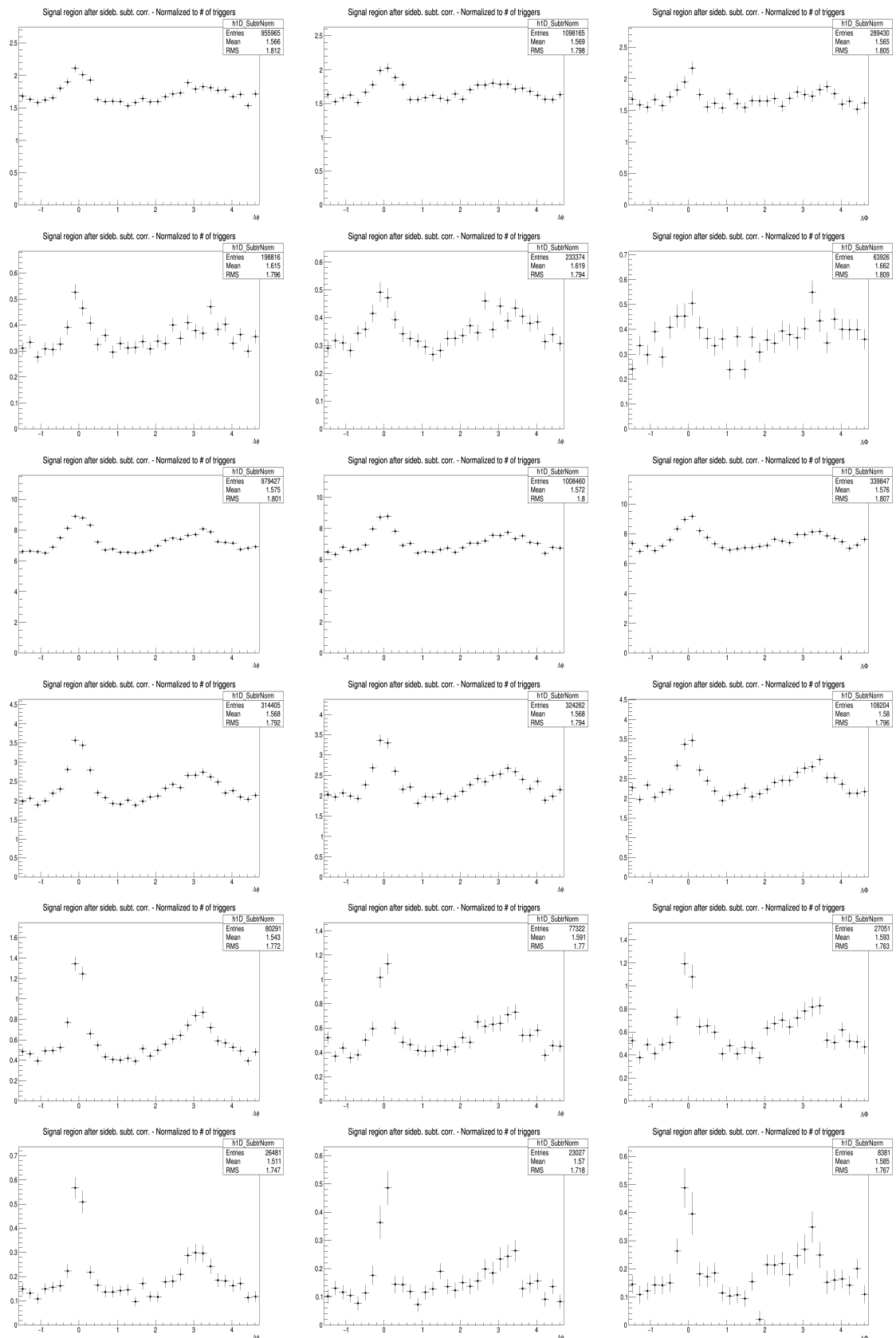
$$\sigma^2 = \frac{\sum_{i=\text{meson}} w_i^2 \sigma_i^2}{(\sum_{i=\text{meson}} w_i)^2} \quad (8)$$

²A slight near side hierarchy is present among the three meson results, with D^{*+} meson having a lower peak amplitude than D^0 and D^+ . It was verified that this is induced by the presence of D^0 and D^+ mesons coming from D^{*+} , the latter having on average a larger p_T and coming, hence, on average, from a larger p_T quark parton, which fragments in slightly more tracks in the near-side.

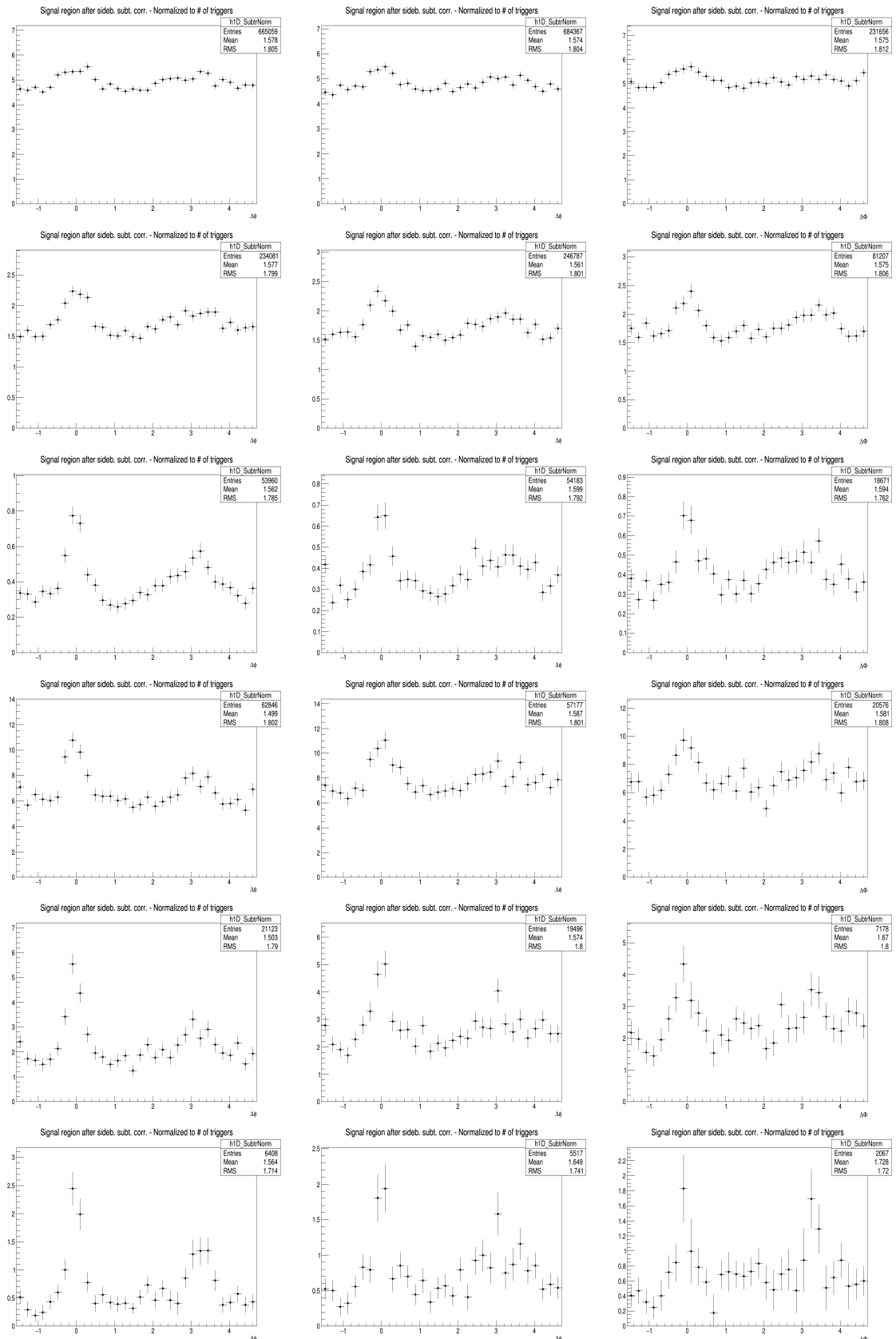


5.2 Average of D^0 , D^+ and D^{*+} results





5.2 Average of D^0 , D^+ and D^{*+} results



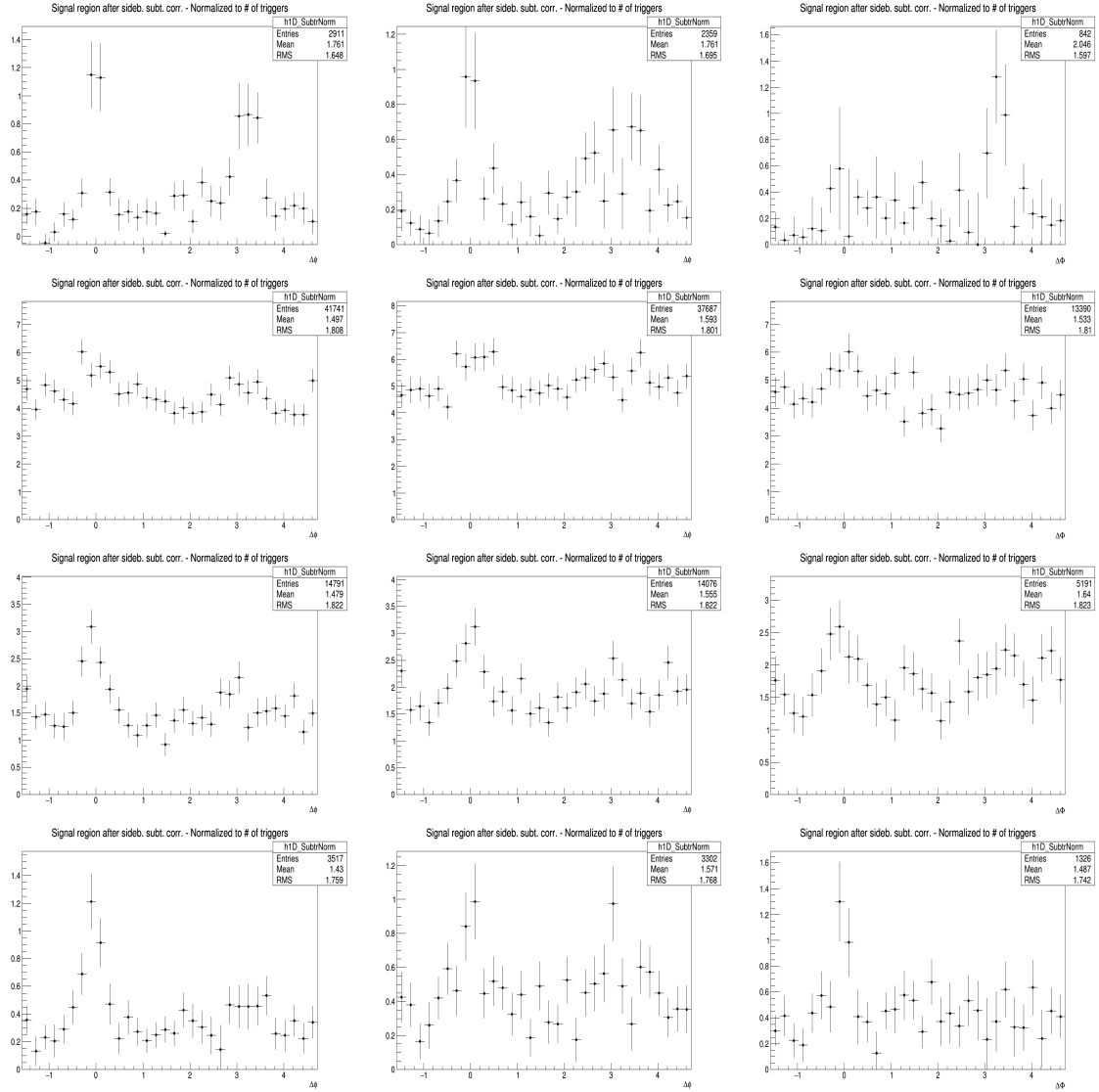
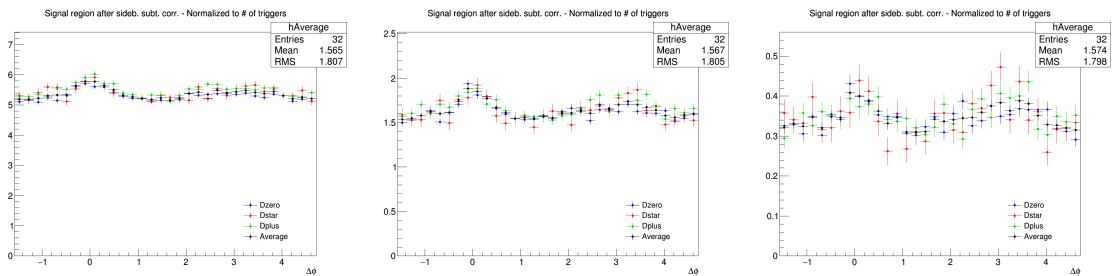
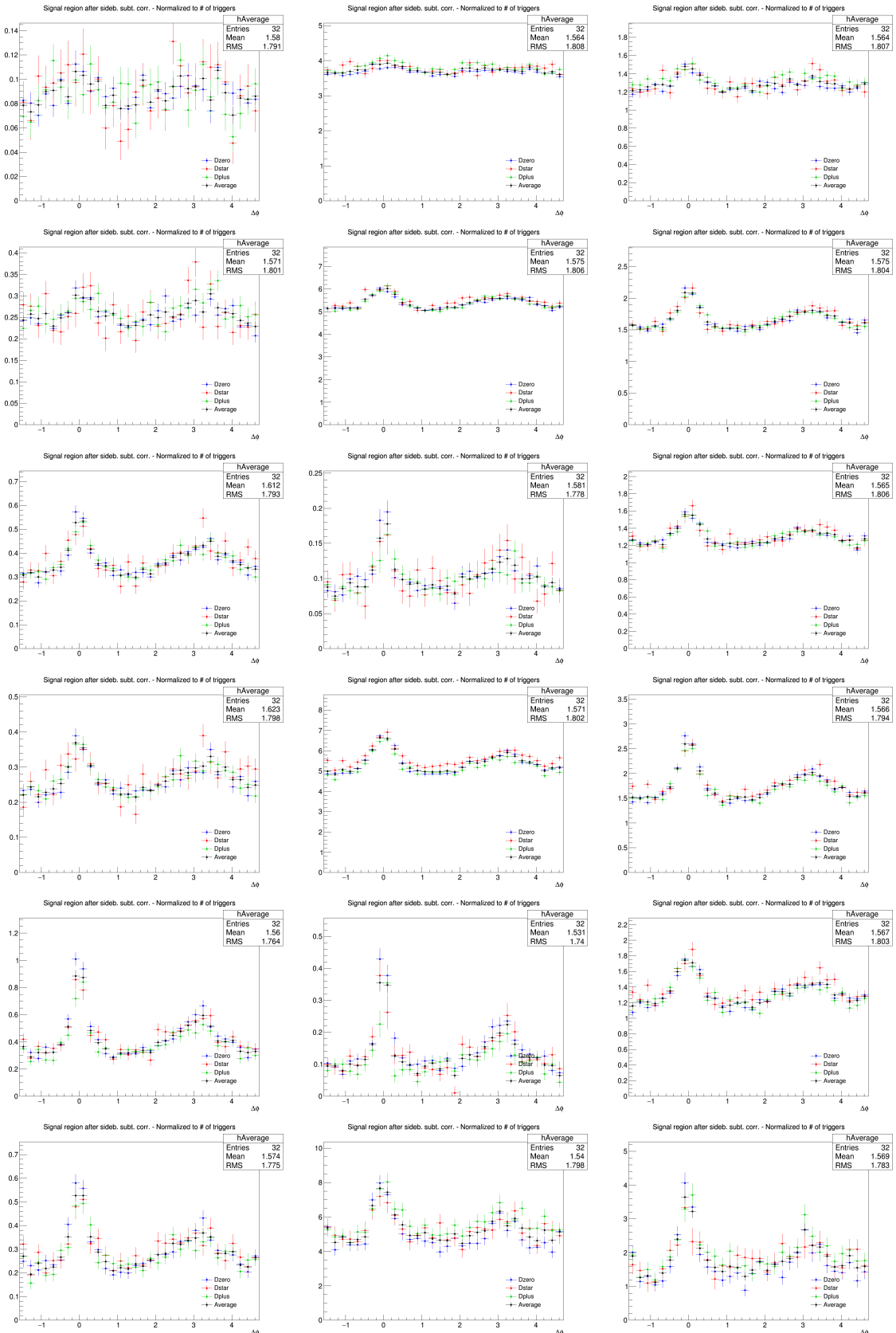


Figure 8: Comparison of the corrected distribution of D-hadrons azimuthal correlations for the three species (apart from feed-down and purity), from analysis on the data sample, for the analyzed D-meson and associated track p_T ranges (Column-Left: $5 < D^0 p_T < 8 \text{ GeV}/c$, Column-Right: $8 < D^0 p_T < 16 \text{ GeV}/c$) and associated tracks p_T ranges (Row1: $>0.3 \text{ GeV}/c$, Row2: $0.3 \text{ to } 1 \text{ GeV}/c$, Row3: $>1.0 \text{ GeV}/c$)



5.2 Average of D^0 , D^+ and D^{*+} results



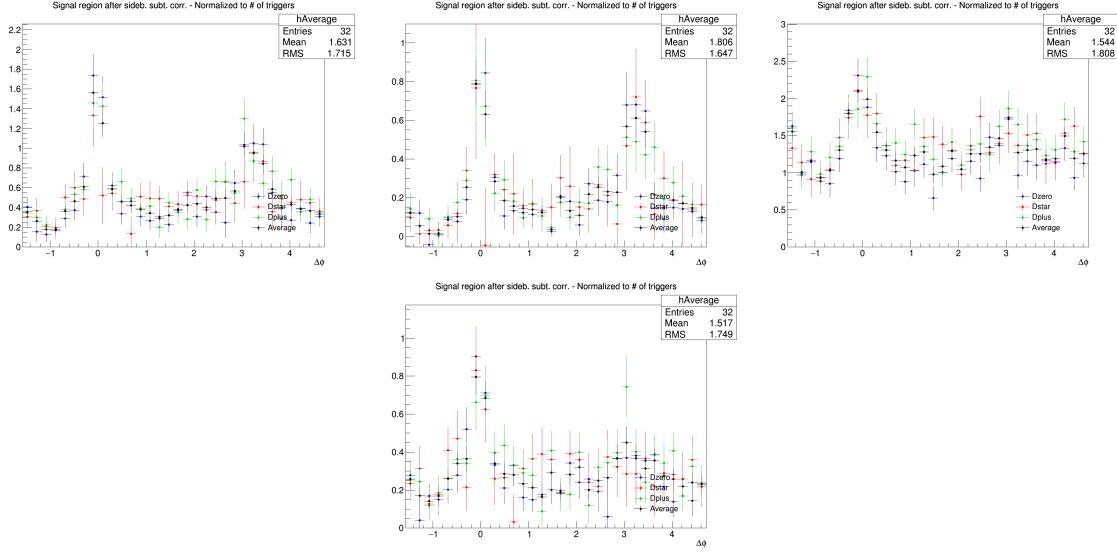


Figure 9: Superimposition of the corrected distribution of D-hadrons azimuthal correlations for the three species (apart from feed-down and purity), from analysis on the data sample, for the analyzed D-meson and associated track p_T ranges (Column-Left: $5 < D^0 p_T < 8 \text{ GeV}/c$, Column-Right: $8 < D^0 p_T < 16 \text{ GeV}/c$) and associated tracks p_T ranges (Row1: $>0.3 \text{ GeV}/c$, Row2: $0.3 \text{ to } 1 \text{ GeV}/c$, Row3: $>1.0 \text{ GeV}/c$)

$$\sigma = \frac{\sum_{i=\text{meson}} w_i \sigma_i}{\sum_{i=\text{meson}} w_i} \quad (9)$$

337 Figure 10 shows the averages of the azimuthal correlation distributions of D^0 , D^+ and D^{*+} and charged
 338 particles with $p_T > 0.3 \text{ GeV}/c$, $0.3 < p_T < 1 \text{ GeV}/c$, $p_T > 1 \text{ GeV}/c$, $1 < p_T < 2 \text{ GeV}/c$, $2 < p_T <$
 339 $3 \text{ GeV}/c$, $p_T < 3 \text{ GeV}/c$, $3 < p_T < 5 \text{ GeV}/c$, $5 < p_T < 8 \text{ GeV}/c$, $8 < p_T <$
 340 $16 \text{ GeV}/c$ and $16 < p_T < 24 \text{ GeV}/c$. As expected, a rising trend of the height of the near-side peak with
 341 increasing D-meson p_T is observed, together with a decrease of the baseline level with increasing p_T of
 342 the associated tracks.

343 The usage of weighted average requires, as an underlying assumption, identical results expected for
 344 different species (or, at least, compatible within the uncertainties).

345 5.3 Nearside associated yield, nearside width and baseline as function of the D meson p_T

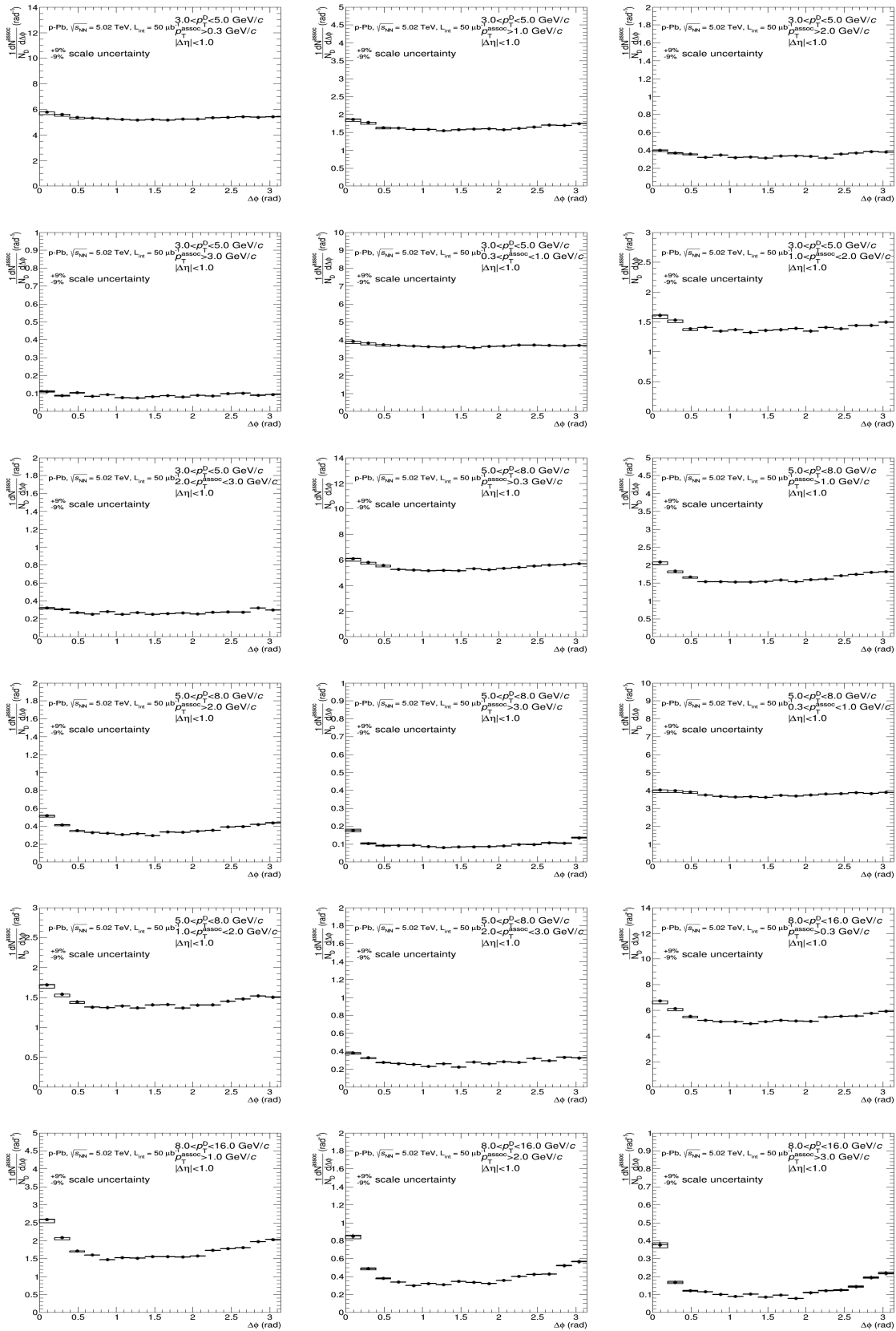
346 In order to extract quantitative and physical information from the data correlation patterns, the averaged
 347 D-h correlation distributions are fitted with two Gaussian functions (with means fixed at $\Delta\phi=0$ and $\Delta\phi=\pi$
 348 values), plus a constant term (baseline). A periodicity condition is also applied to the fit function to obtain
 349 the same value at the bounds of 2π range. The expression of the fit expression is reported below (equation
 350 10):

$$f(\Delta\phi) = c + \frac{Y_{NS}}{\sqrt{2\pi}\sigma_{NS}} e^{\frac{(\Delta\phi-\mu_{NS})^2}{2\sigma_{NS}^2}} + \frac{Y_{AS}}{\sqrt{2\pi}\sigma_{AS}} e^{\frac{(\Delta\phi-\mu_{AS})^2}{2\sigma_{AS}^2}} \quad (10)$$

351 where baseline is calculated as the weighted average of the points lying in the so-called "transverse
 352 region", i.e. the interval $\frac{\pi}{4} < |\Delta\phi| < \frac{\pi}{2}$.

353 An example of the results from the fit is shown in Figure 11

354 From the fit outcome is it possible to retrieve the near-side and away-side yield and widths (integral and
 355 sigma of the Gaussian functions, respectively), as well as the baseline height. The near-side observables



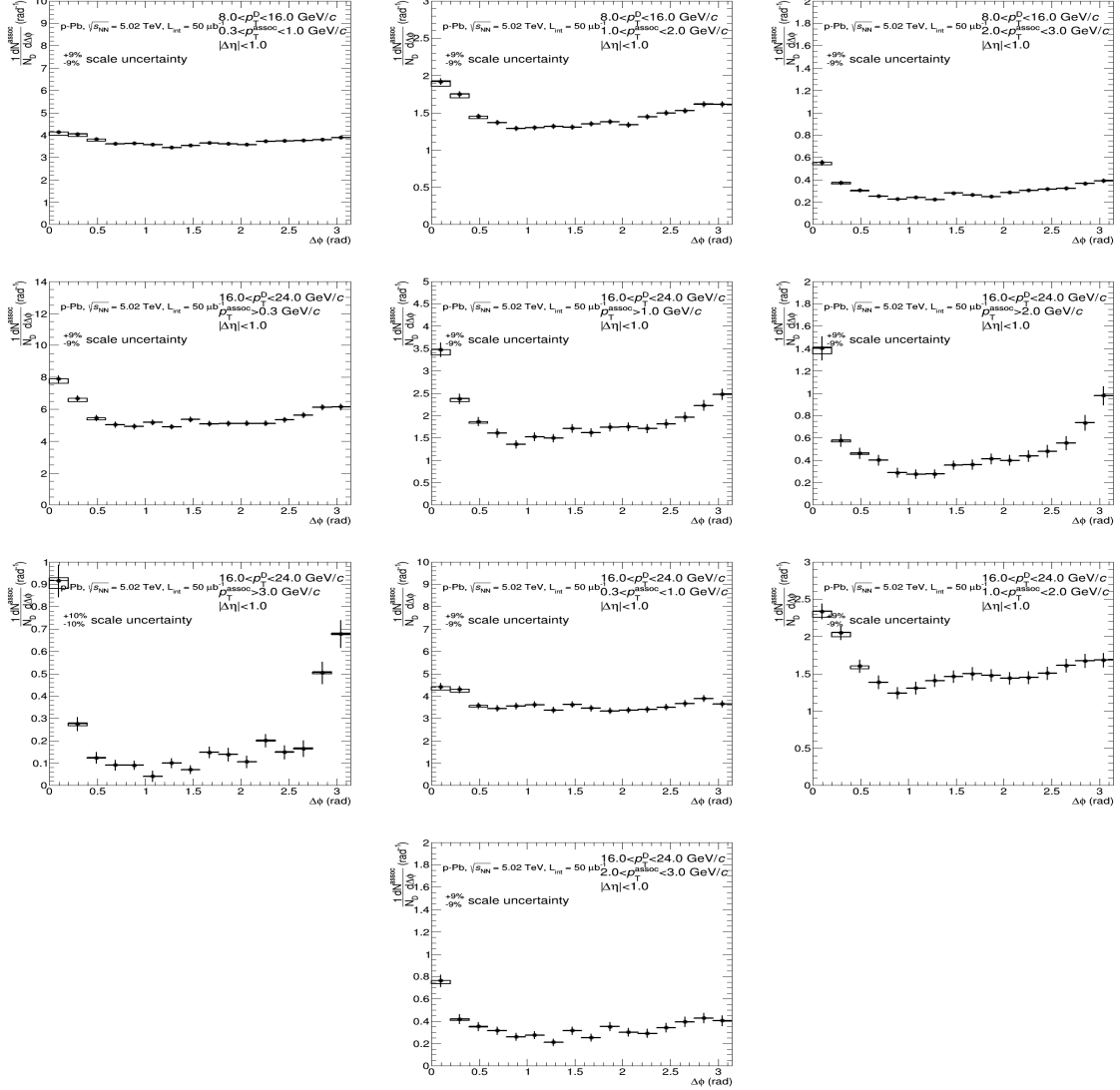


Figure 10: Average of D^0 , D^+ and D^{*+} azimuthal correlation distributions, in the D meson p_T ranges $5 < p_T < 8 \text{ GeV}/c$ and $8 < p_T < 16 \text{ GeV}/c$, with associated tracks with $p_T > 0.3 \text{ GeV}/c$, $p_T > 1 \text{ GeV}/c$ and $0.3 < p_T < 1 \text{ GeV}/c$.

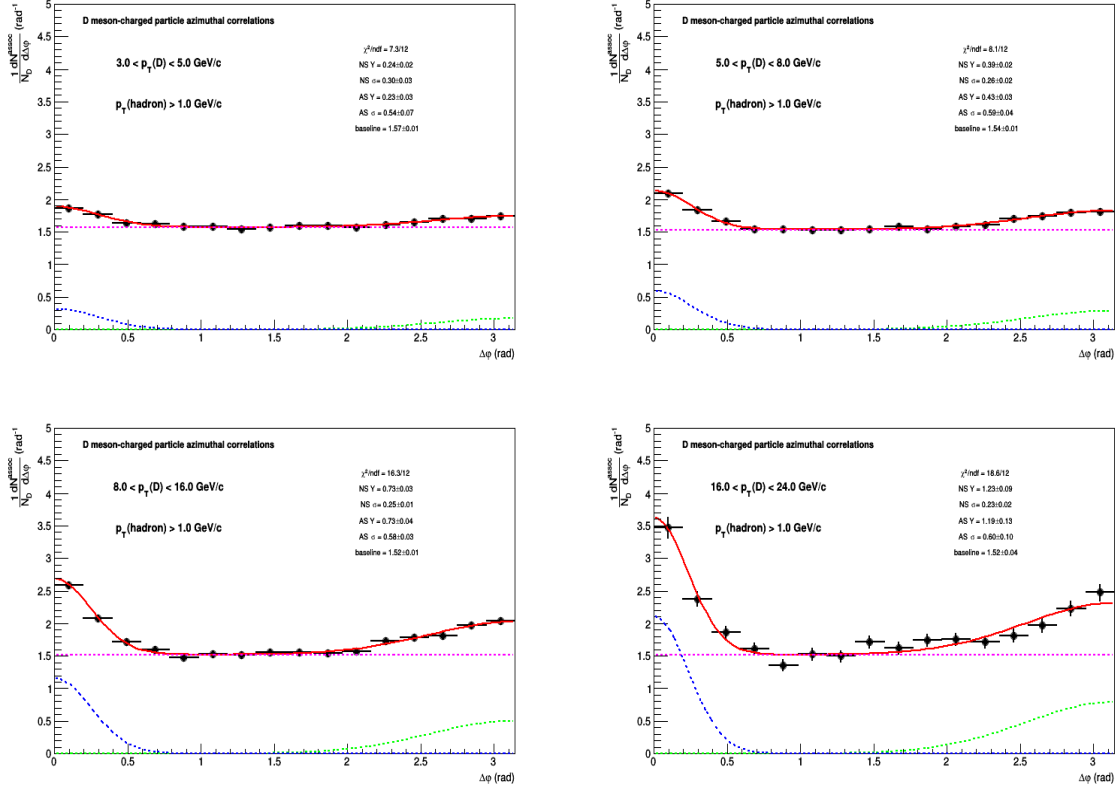


Figure 11: Example of fit to azimuthal correlation distributions and baseline estimation.

give information on the multiplicity and angular spread of the tracks from the fragmentation of the charm jet which gave birth to the D-meson trigger, while at first order the away-side observables are related to the hadronization of the charm parton produced in the opposite direction (though the presence of NLO processes for charm production breaks the full validity of this assumption). The baseline value is a rough indicator of the underlying event multiplicity, though below the baseline level also charm and beauty-related pairs are contained (especially in cases of NLO production for the heavy quarks).

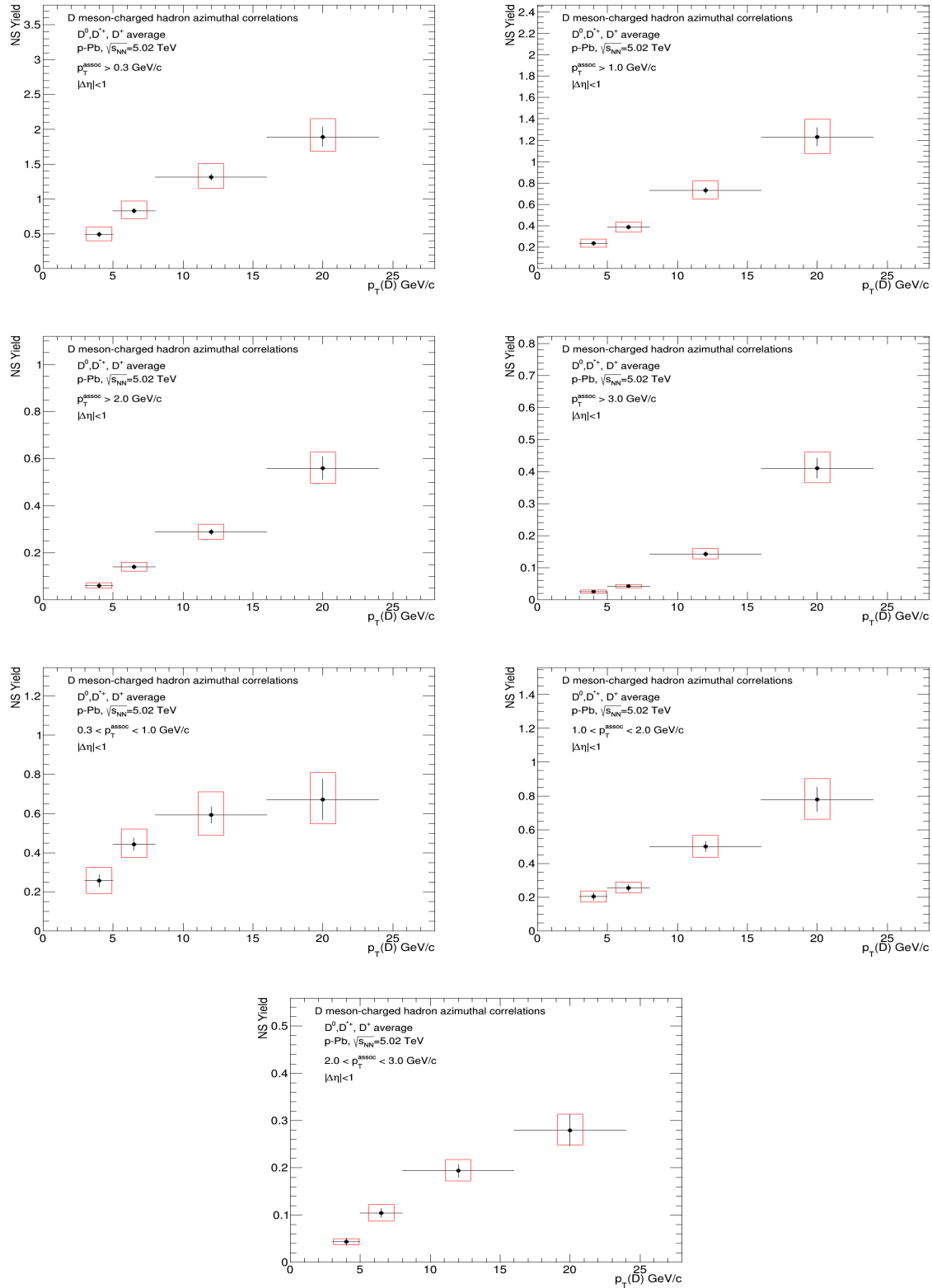
The evaluation of the systematic uncertainties on the observables obtained from the fits is performed as follows:

- The fits are repeated by changing the range of the transverse region in which the baseline is evaluated. Alternate definitions of $\frac{\pi}{4} < |\Delta\phi| < \frac{3\pi}{8}$, $\frac{3\pi}{8} < |\Delta\phi| < \frac{\pi}{2}$ and $\frac{\pi}{4} < |\Delta\phi| < \frac{5\pi}{8}$ are considered.
- In addition, $\Delta\phi$ correlation points are shifted to the upper and lower bounds of their uncorrelated systematic boxes, and the refitted.
- The maximum variation of the parameters between the fit outcomes defined in the previous points is considered as systematic uncertainty for the near-side and away-side widths.
- For the estimation of the baseline and of the near-side and away-side yields, the previous value is added in quadrature with the $\Delta\phi$ -correlated systematics in the correlation distributions, since these values are affected by a change in the global normalization of the distributions.

$$\sigma_{\text{syst}}^{\text{syst}} = \sqrt{(\text{Max}(\Delta\text{par}^{\text{ped.mode}}, \Delta\text{par}^{\Delta\phi\text{point}}))^2 + (\sigma_{\text{Syst}}^{\text{corr}})^2} \quad (11)$$

373 **5.3.1 Results for near-side yield, near-side width and baseline**

374 Figures 12, 13, 15, 15 and 16 show the near-side associated yield, width (the sigma of the Gaussian
375 part of the fit functions) and the height of the baseline, for the average correlation distributions, in the
376 kinematic ranges studied in the analysis. For each kinematic range, the correspondent plot showing the
377 systematic uncertainty of the considered observable from the variation of the fit procedure is reported
378 as well (which is the full systematic uncertainty for the widths). Figures ??, ??, and 19 show the full
379 systematic uncertainties for yields and baseline, with the breakdown of fit variation and $\Delta\phi$ correlated
380 systematic uncertainties.



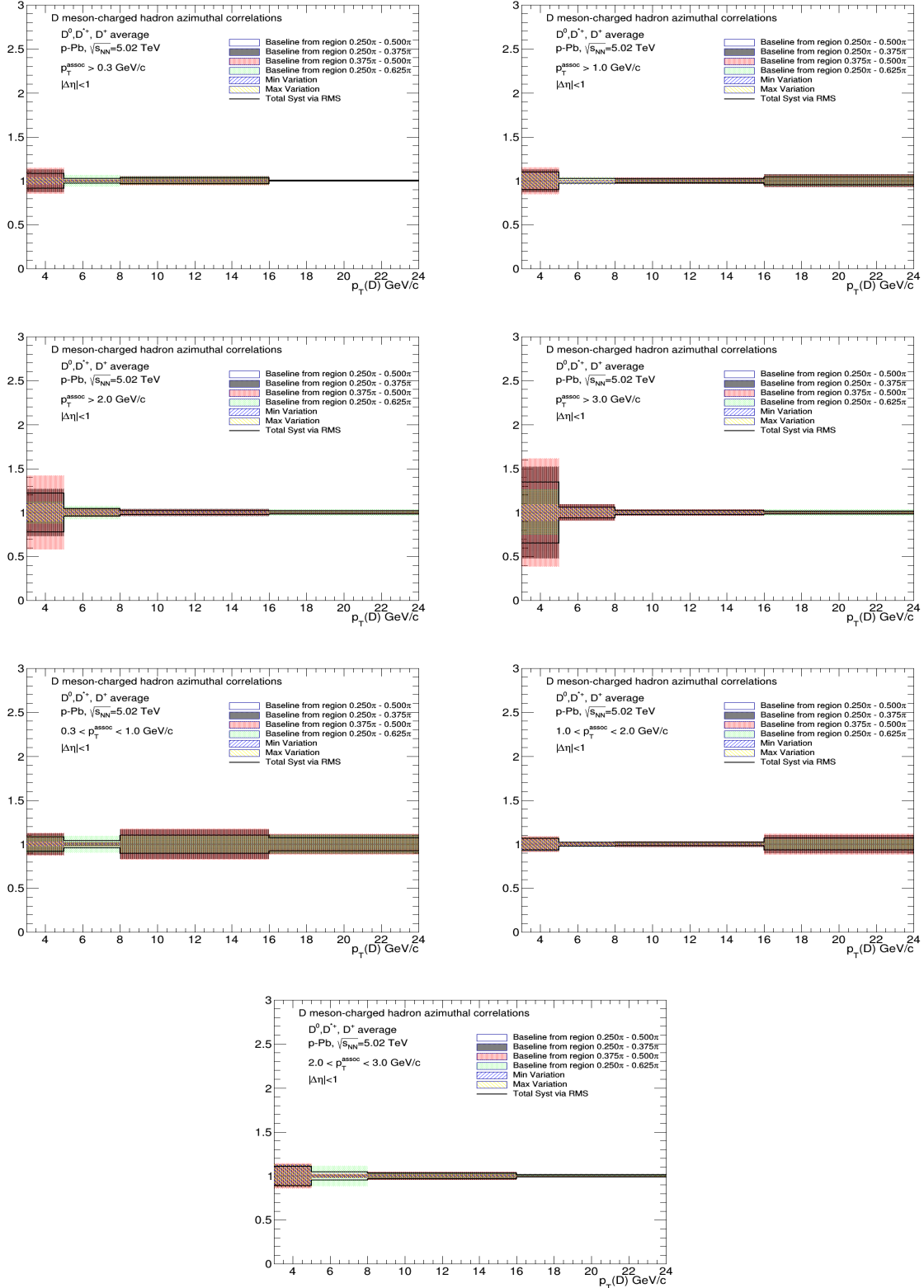
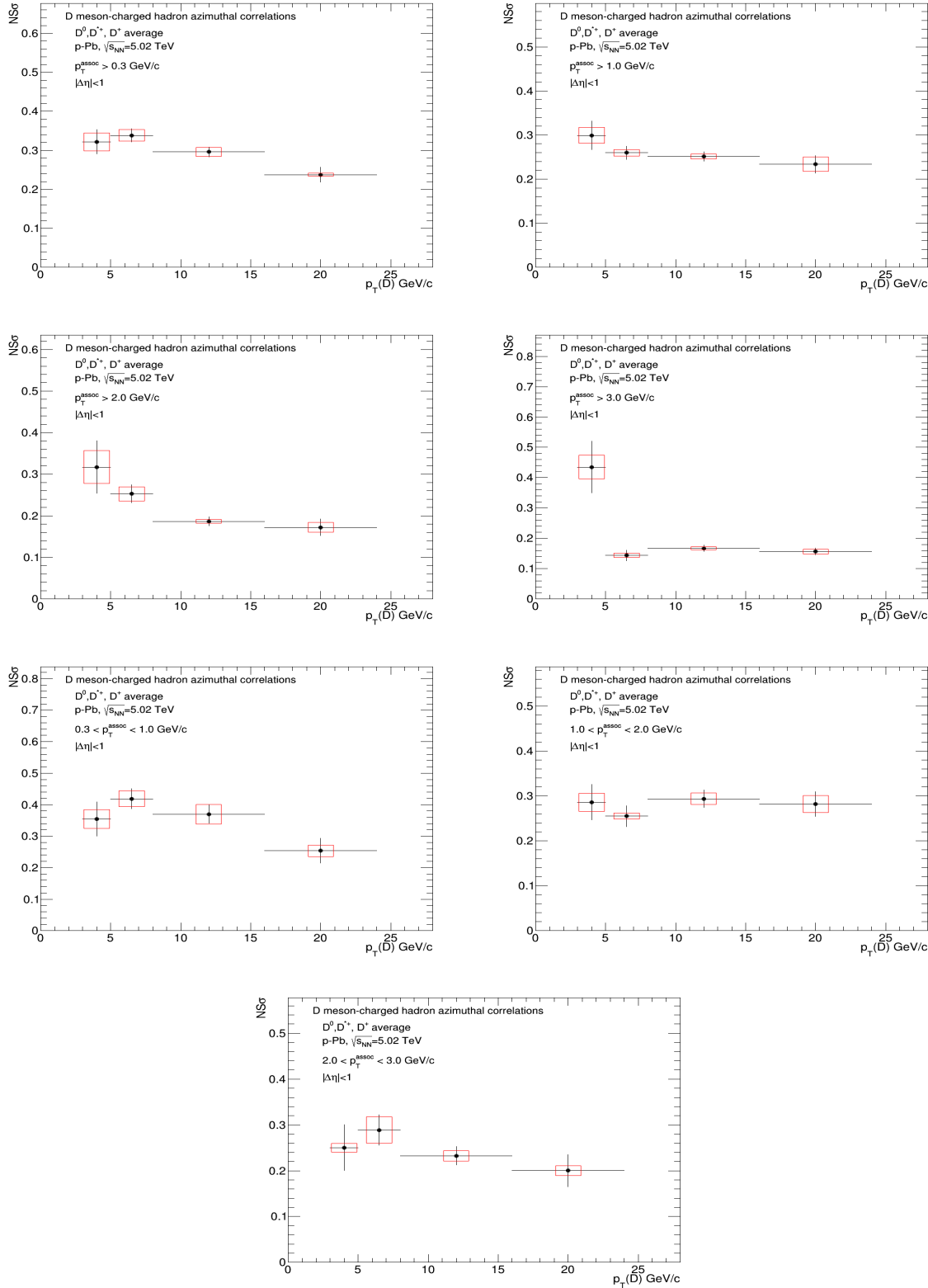


Figure 12: Near side yield $p_T(D)$ trend for the D-meson average, extracted from fit to the azimuthal correlation distributions, for all the analyzed kinematic ranges of associated track p_T . In the right column, for each kinematic region the systematic uncertainties coming from the variation of the fit procedure are shown.



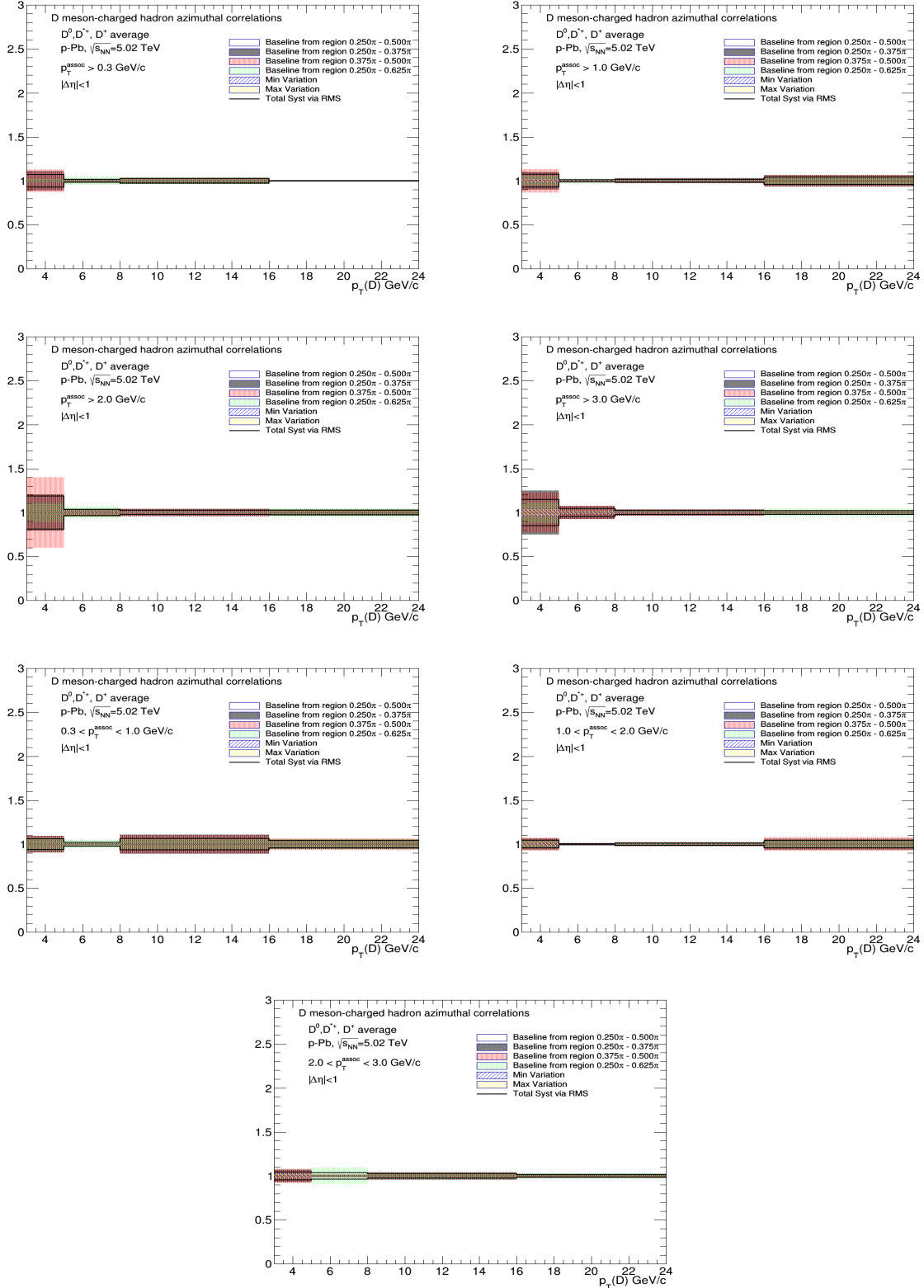
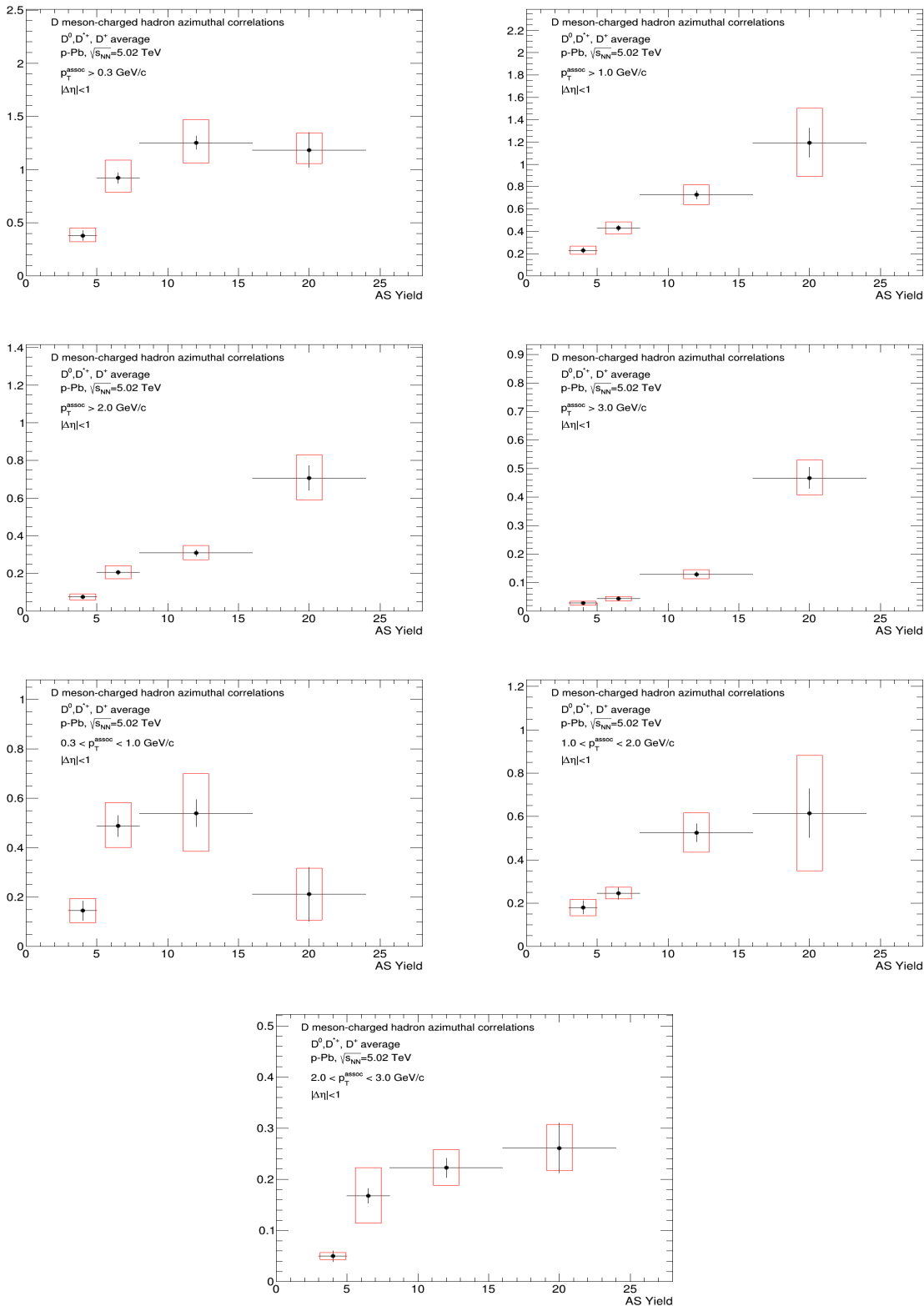


Figure 13: Near side width $p_T(D)$ trend for the D-meson average, extracted from fit to the azimuthal correlation distributions, for all the analyzed kinematic ranges of associated track p_T . In the right column, for each kinematic region the systematic uncertainties coming from the variation of the fit procedure are shown.



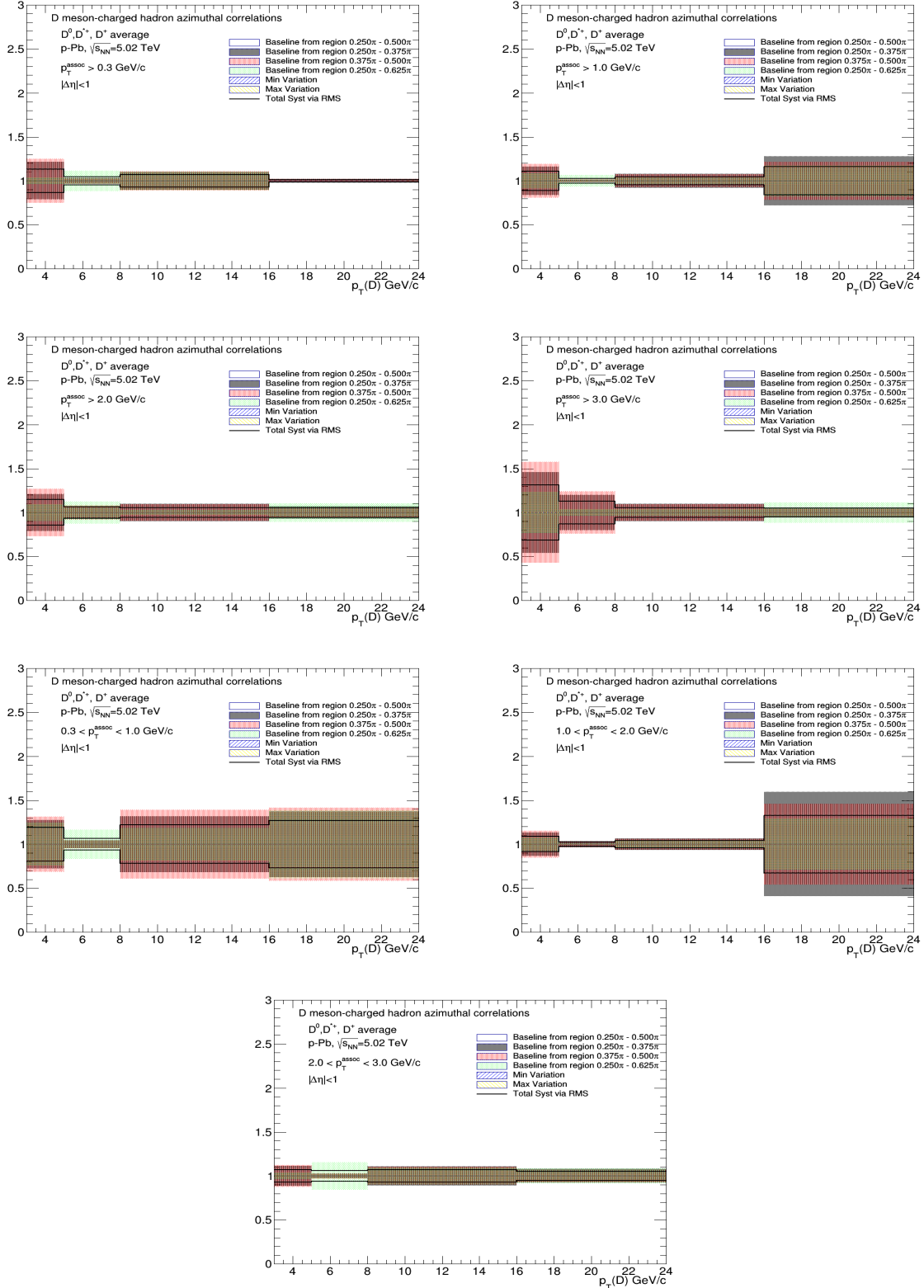
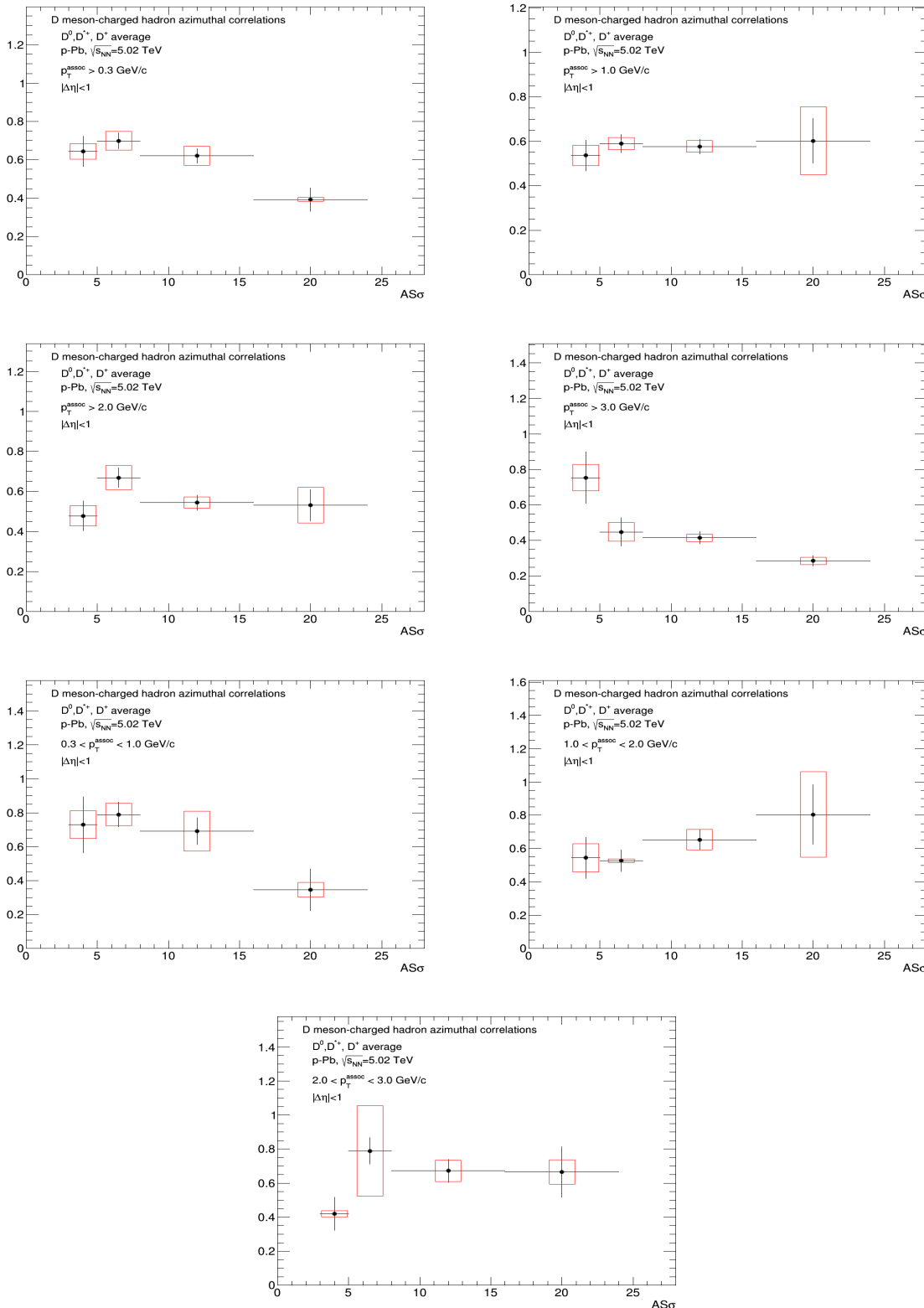


Figure 14: Away side yield $p_T(D)$ trend for the D-meson average, extracted from fit to the azimuthal correlation distributions, for all the analyzed kinematic ranges of associated track p_T . In the right column, for each kinematic region the systematic uncertainties coming from the variation of the fit procedure are shown.



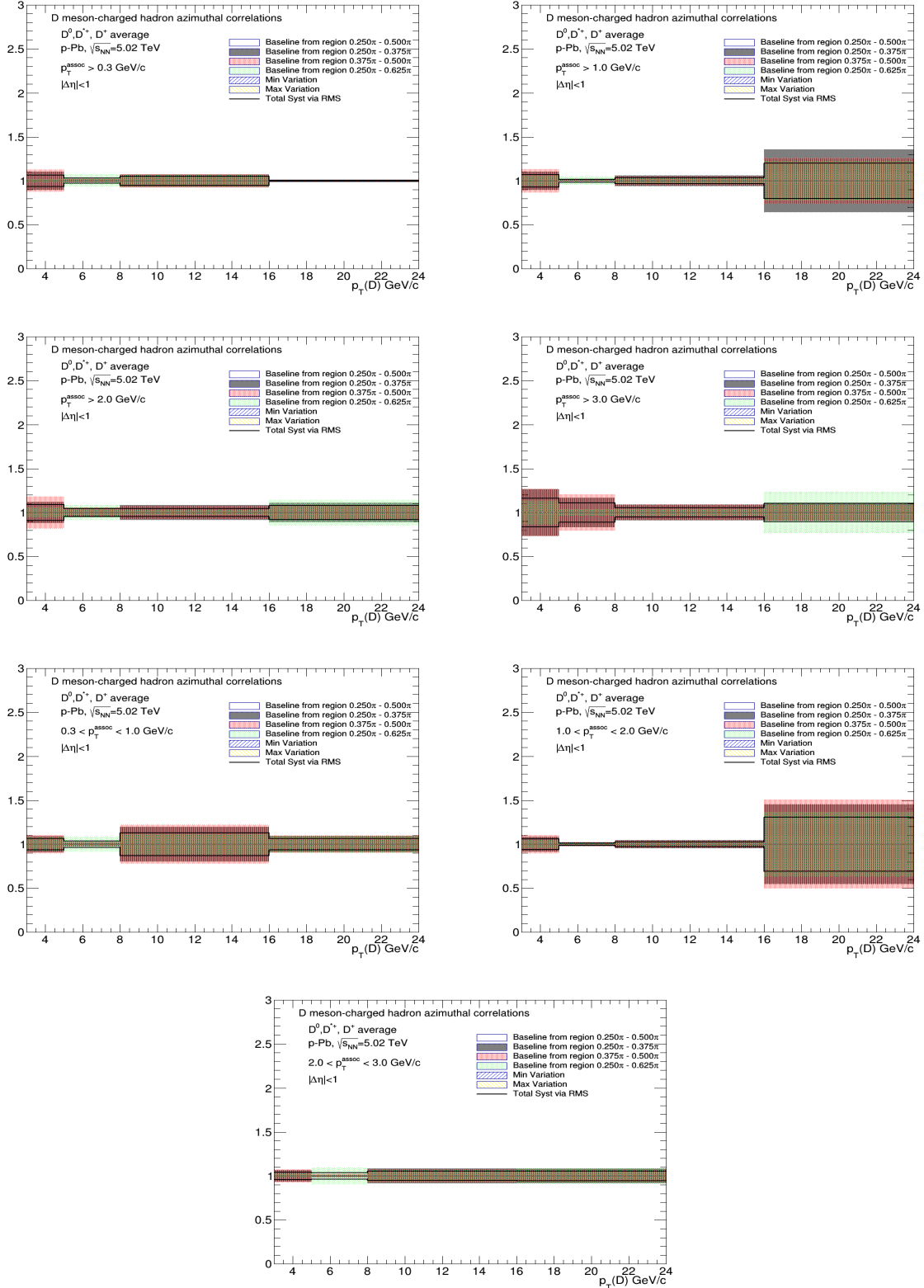
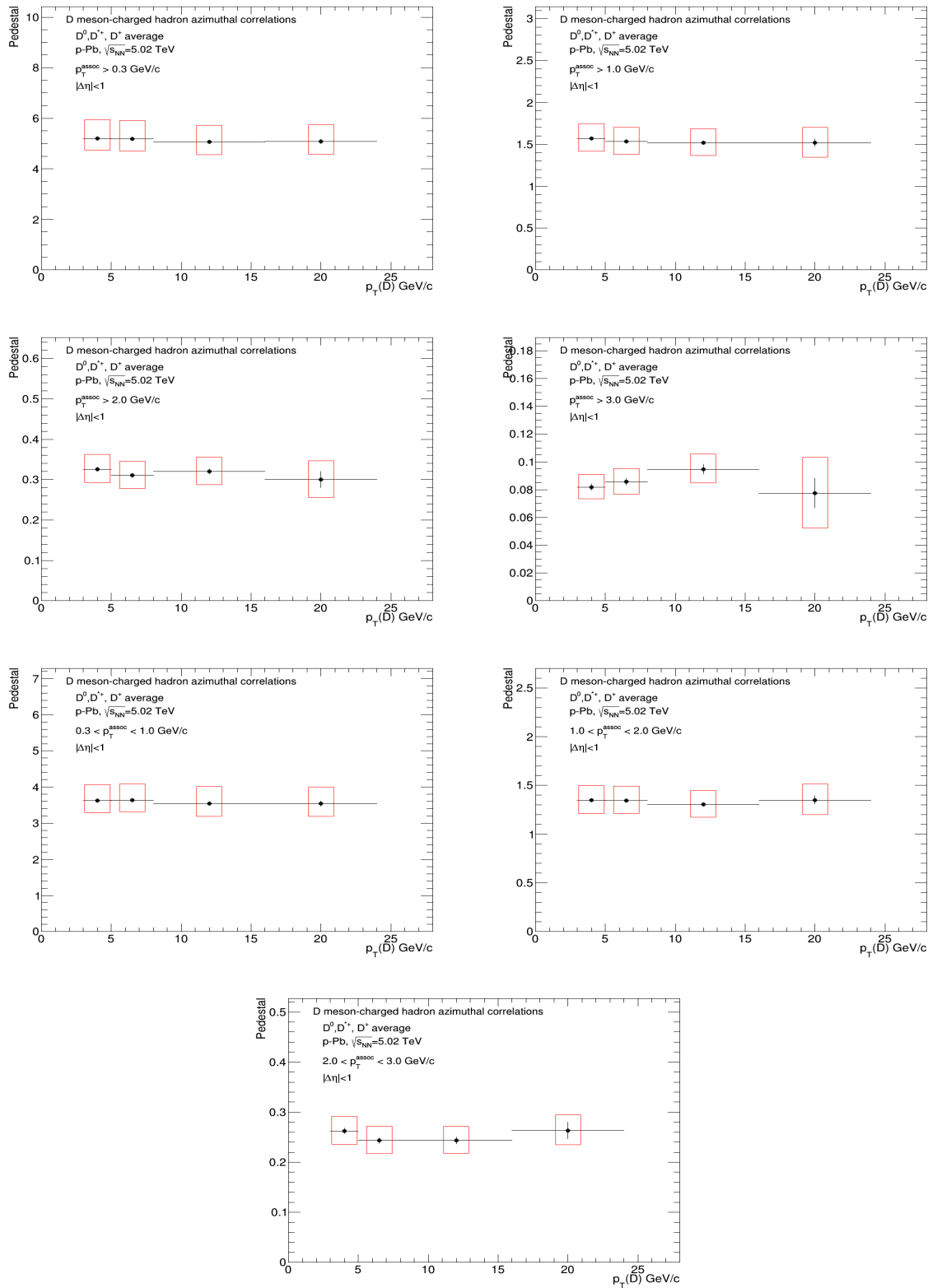


Figure 15: Away side width $p_T(D)$ trend for the D-meson average, extracted from fit to the azimuthal correlation distributions, for all the analyzed kinematic ranges of associated track p_T . In the right column, for each kinematic region the systematic uncertainties coming from the variation of the fit procedure are shown.



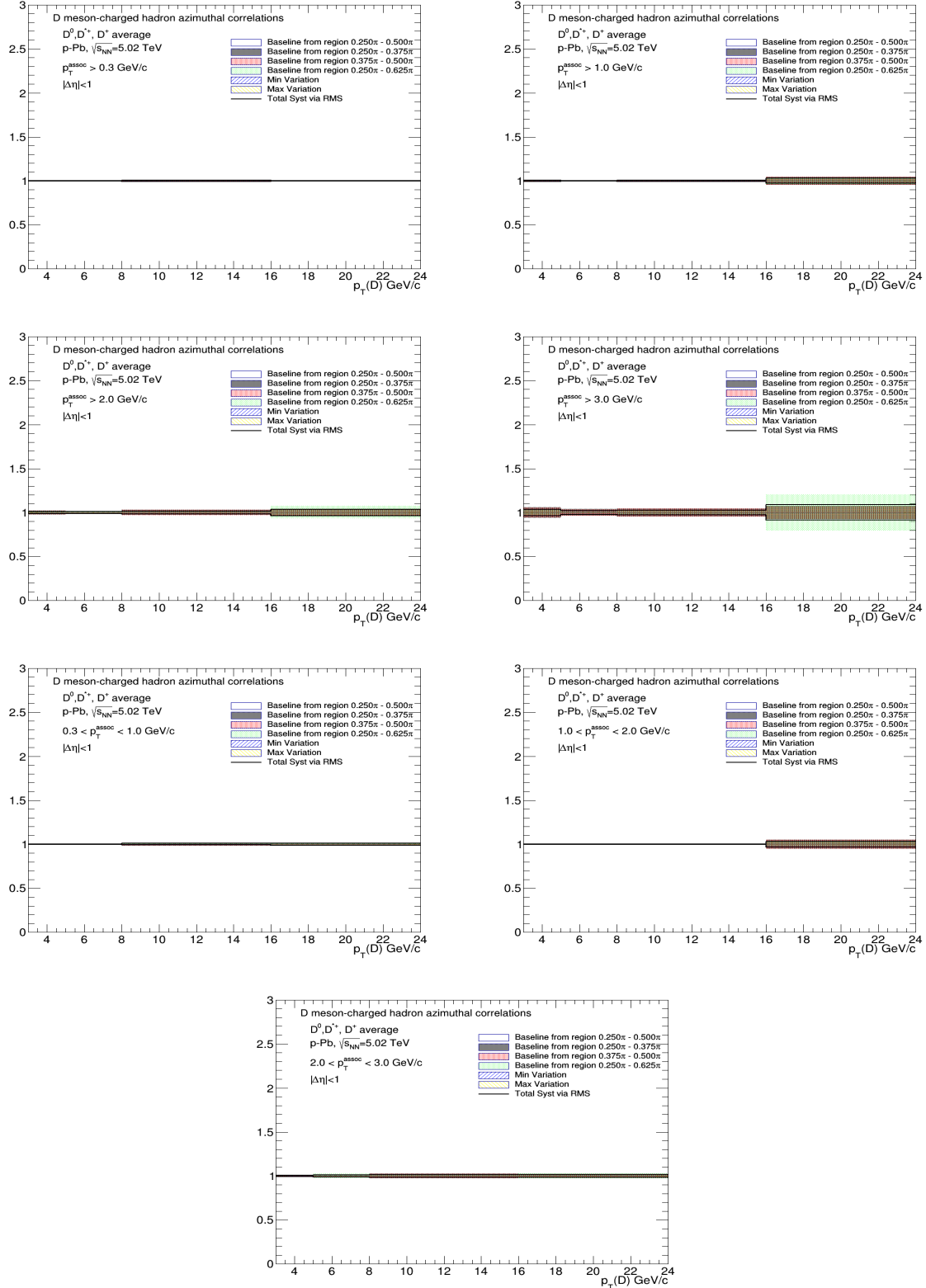


Figure 16: Baseline height trend for the D-meson average, extracted from fit to the azimuthal correlation distributions, for all the analyzed kinematic ranges of associated track p_T . In the right column, for each kinematic region the systematic uncertainties coming from the variation of the fit procedure are shown.

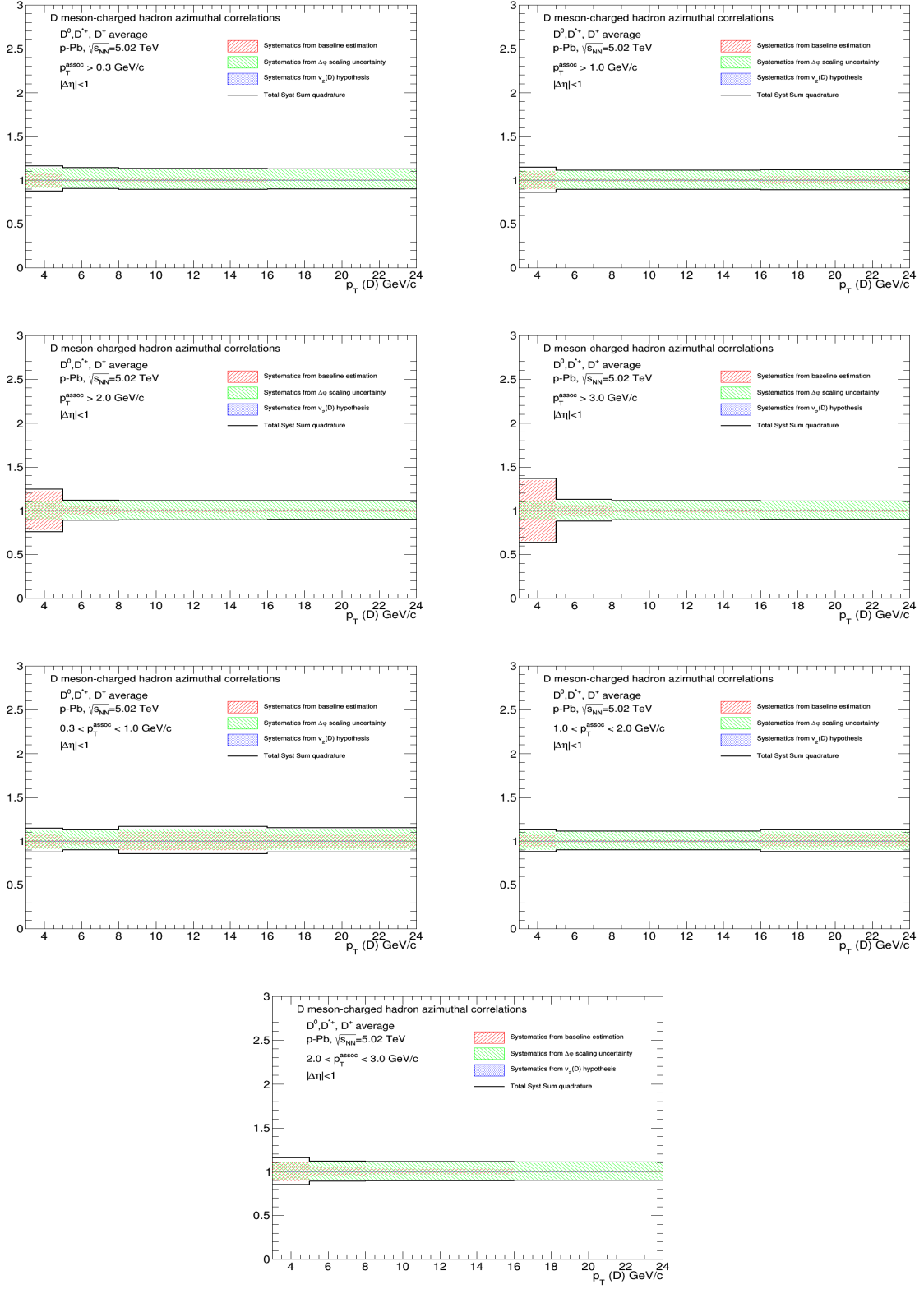


Figure 17: Total systematic uncertainty, and its component, for near-side yields in the different kinematic ranges analyzed

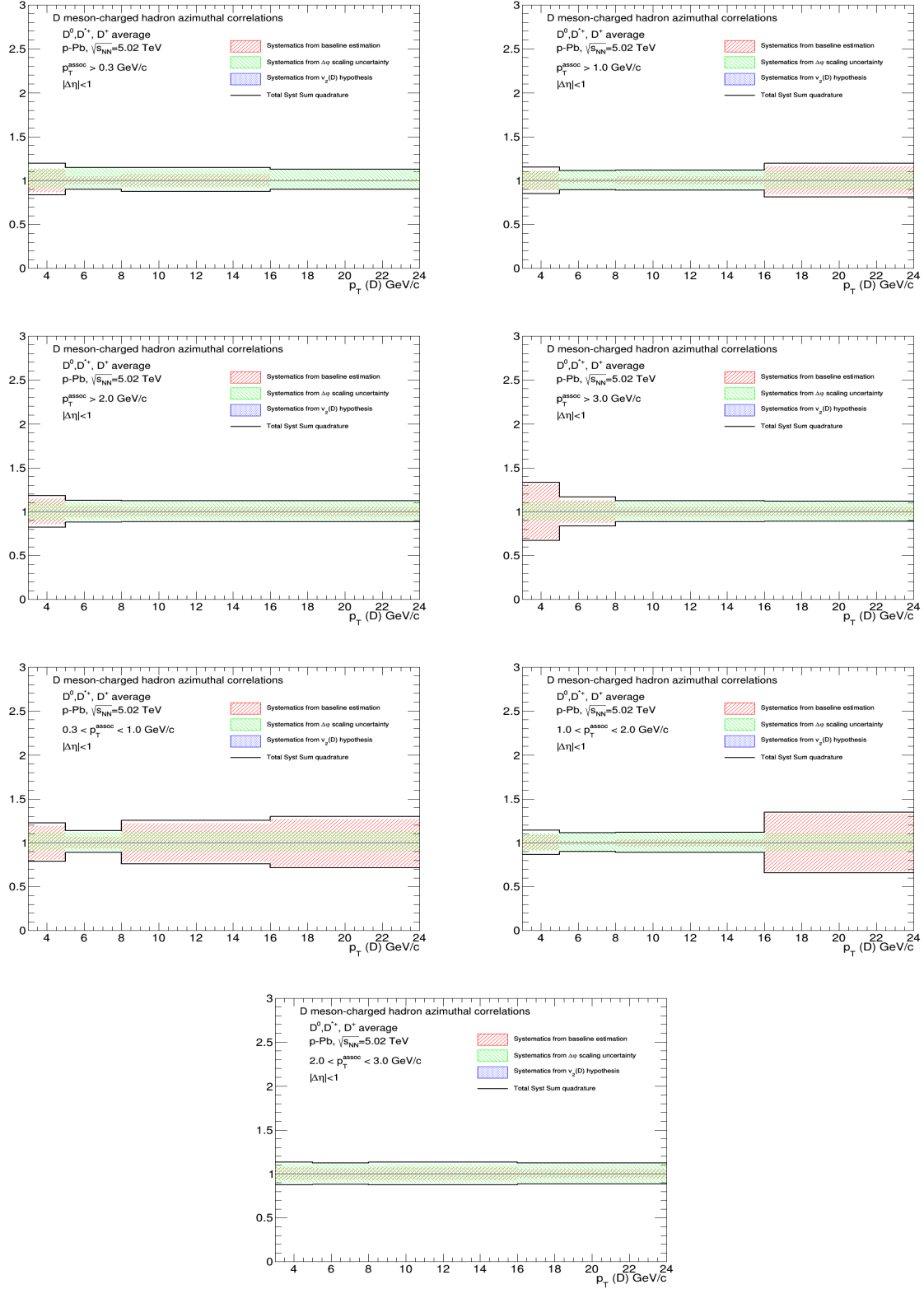


Figure 18: Total systematic uncertainty, and its component, for away-side yields in the different kinematic ranges analyzed

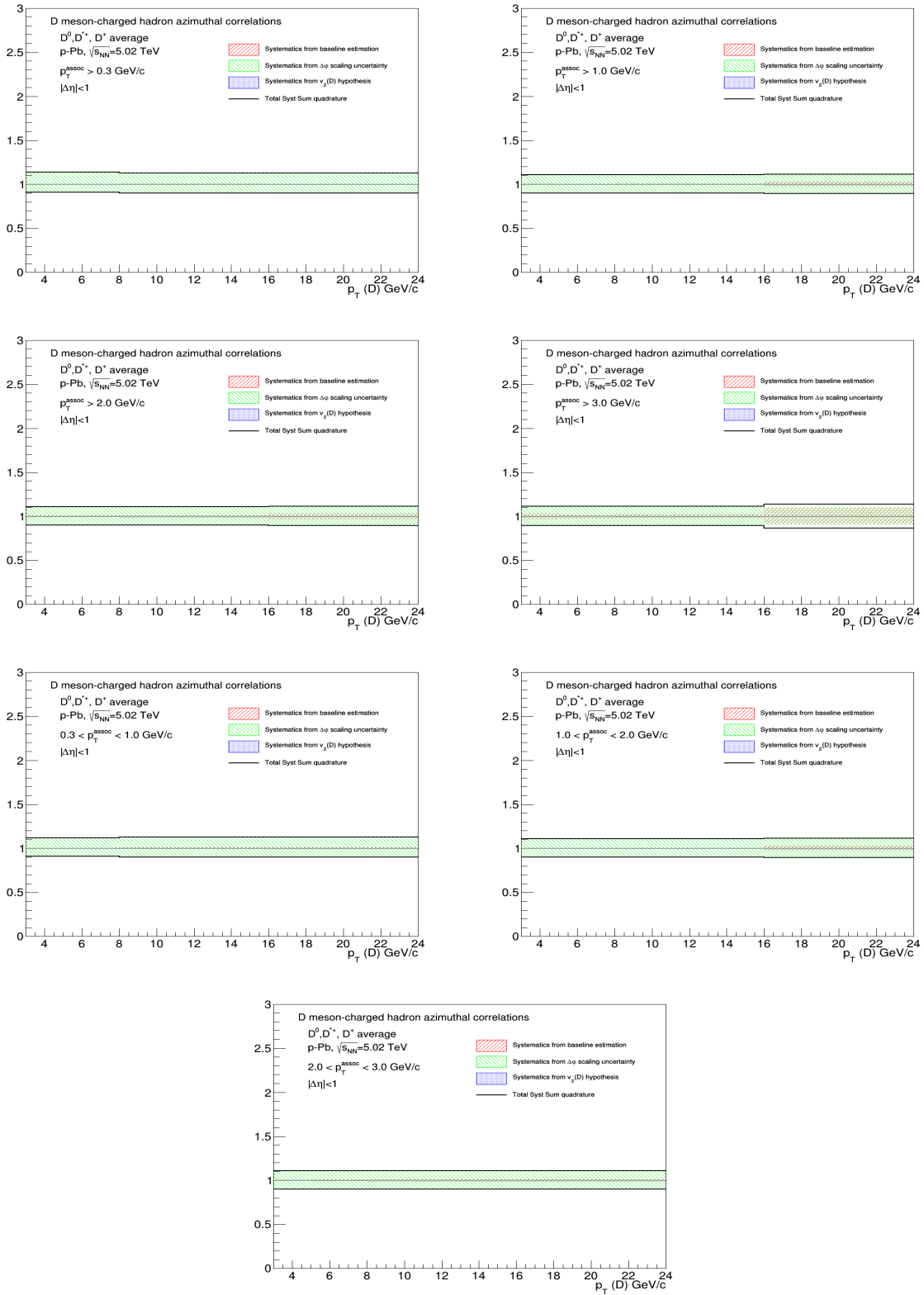


Figure 19: Total systematic uncertainty, and its component, for baseline heights in the different kinematic ranges analyzed.

381 **6 Conclusions**

382 text

383 **7 Bibliography**

384 **References**

- 385 [1] J. Adam et al. [ALICE Collaboration], Nature Physics (2017) doi:10.1038/nphys4111.
386 [2] [E791 Collaboration], Correlations between D and \bar{D} mesons produced in 500GeV π -nucleon in-
387 teractions; EPJdirect C1 (2008)
388 [3] [CDF Collaboration], Measurement of Charm Meson pair Cross Section; CDF-Note 8621 2006.
389 [4] X.Zhu, N.Xu, P.Zhuang, Phys.Rev.Lett.100:152301,2008, arXiv:0709.0157.
390 [5] M. Nahrgang, J. Aichelin, P. B. Gossiaux, K. Werner, arXiv:1305.3823.
391 [6] B. Abelev et al. [ALICE Collaboration], JHEP **01** (2012) 128.